UNIVERSITY
OF TRENTO - Italy
Department of Physics

CONFINDUSTRIA TRENTO

POLO
MECCATRONICA

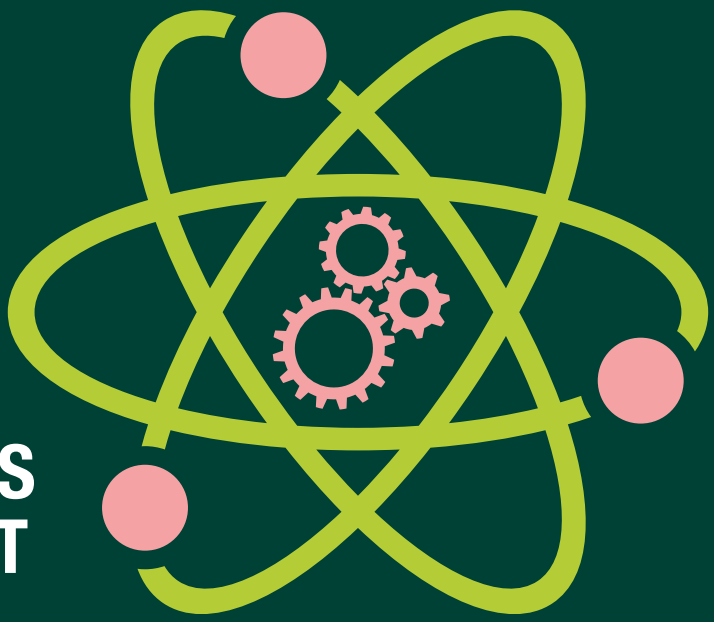

PROCEEDINGS OF THE EVENT IPSP2018 INDUSTRIAL PROBLEM SOLVING WITH PHYSICS

Trento (Italy)
July 16-21, 2018

UNIVERSITY
OF TRENTO - Italy
DEPARTMENT OF PHYSICS

Proceedings of the event IPSP2018

Industrial Problem Solving with Physics
Trento, July 16 – 21, 2018

Editors
Zahra Bisadi
Sofia Colombi
Matteo Di Giovanni

Trento
Università degli Studi di Trento

Proceedings of the event IPSP2018: Industrial Problem Solving with Physics: Trento, July 16 – 21, 2018 / editors Zahra Bisadi, Sofia Colombi, Matteo Di Giovanni. - Trento: Università degli Studi di Trento, 2018. - 71 p.: ill. - ISBN: 978-88-8443-823-2.

Latex class available at `https://github.com/mrgrass/IPSP_latex_Class`

PREFACE

Confindustria Trento is a partner of IPSP since the very first edition. When the founders of the competition – three PhD students of the Physics Department of the University of Trento – presented us their idea, we decided to join the project mainly for three reasons. First of all, it is a bottom-up initiative managed by proactive students. Second, it contributes to promote the role of graduates and PhDs in Physics within the industrial sector. Third, it can really help to narrow the gap between research and industry.
So far, our experience with IPSP has been extremely positive. Companies who participated in IPSP have obtained innovative solutions to their technical problems, with important effects on their products and productive processes. That is why we will support IPSP in the future as well. Let's innovate together!

Alessandro Santini, Confindustria Trento

Since its founding in 1986, Trentino Sviluppo has been promoting the connection between research, business and education. On these pillars we built Polo Meccatronica, a technology hub where companies, students and researchers work side by side to face the challenges posed by Industry 4.0. Technology transfer, innovation and cross-fertilization are also the basis of ProM Facility, our cutting-edge laboratory where SMEs, industrial groups, startups and researchers develop and patent new business ideas related to the additive manufacturing and prototyping fields.
Recognizing the importance of the circular transfer of knowledge, we are therefore proud to renew our commitment to the IPSP initiative. To us, this competition represents a gainful opportunity for both young talents – who can test their academic skills on the ground – and enterprises – which can experiment innovative solutions to achieve their goals as well as make contact with the most brilliant physicists of the future. Finally, we wish luck and success to the new 2019 edition!

Paolo Gregori, Polo Meccatronica

Industrial Problem Solving with Physics has reached its 5th edition in 2018 and from a Technology Transfer perspective it has consolidating a new model of industry-academia collaboration which allows industrial problems to be solved quickly and effectively in one week. A growing trend within the initiative consists of a series of meetings among the University and the enterprises involved in IPSP after the event, fostering long term collaborations encouraged by the contribution of Trentino Sviluppo – Polo Meccatronica and Confindustria Trento. Indeed, one of the main targets of IPSP is the development of a strong link between University laboratories and enterprises. Both applied research and placement of young scientists can profit from the dialogue promoted by this event.

Vanessa Ravagni, Research and Technology Transfer Support,
University of Trento

INTRODUCTION

Industrial Problem Solving with Physics (IPSP) is an event organized by the Department of Physics, the Doctoral School of Physics and the Research and Technology Transfer Support Division of the University of Trento, in collaboration with Confindustria Trento and Trentino Sviluppo - Polo Meccatronica. The main objective of this initiative is to promote the collaboration between the Department of Physics and the industrial world.
The first edition of IPSP was launched in 2014 based on the idea of three PhD students who were inspired by "Physics with Industry" organized in the Netherlands. The three PhD students formed the "Scientific Committee" of IPSP which has been an important element in this initiative until today. The huge success of IPSP since 2014 motivated the organization of its fifth edition (IPSP 2018) this year.
IPSP has a *market-oriented* or *active* model and is composed of problems, which are proposed by companies, and participants ("brains"). During one week, the brains (master or PhD students, post-docs and researchers) try different ideas and various approaches to solve the problems and on the final day of the event present their solutions. The proposed solutions have been helpful and practical in all editions. The strengths of IPSP include the efficient format, the presence of young brains on the one hand and companies experiences on the other one and lots of team spirit. In addition, it has successfully promoted the physicists (scientists) in industries and paved the path for more collaboration with them through industrial projects, doctorate scholarships and traineeship possibilities for undergraduate and graduate students. It has also been an exemplar for some similar initiatives organized by other departments of the University of Trento or by innovation-oriented organizations.
This book contains the proceedings of IPSP2018 and describes in detail the activities carried out by the three teams. It is organized in three chapters, each of which begins with a brief overview of the company and a description of the proposed problem, followed by the undertaken strategies, the technical procedures and the final solutions. At the end of each chapter suggestions and conclusions are presented.

Zahra Bisadi, Sofia Colombi, Matteo Di Giovanni

CHAPTER

ONE

THERMODYNAMIC CHARACTERIZATION AND DESIGN OF AN OPTIMAL COOLING SYSTEM FOR AN 18 MJ SUPER CAPACITORS UPS

D. Bazzanella, S. Colombi, R. Franchi, A. Nardin, J. Nespolo, M. Salvagni, M. Scalet, and N. Tubini

1.1 Introduction

1.1.1 Company Profile

Ducati Energia owns its fame to the Ducati brothers who established Ducati company in 1926; 22 years later, Ducati was split in two other companies, Ducati Elettrotecnica and Ducati Meccanica (today Ducati Motor).
It was founded in 1985 due to the merge of Ducati Elettrotecnica and Zanussi Elettromeccanica and nowadays it is considered one of the most important companies in the Bologna area.
Ducati Energia Group assets a staff list of about 900 employees working in its 9 worldwide plants. The main fields of activities are the following: capacitors, power factor correction and power electronics, wind power generators, alternators and ignition systems, electrical vehicles and charging stations, energy analysers, electric network tele-control systems, railway signalling systems, ticket issuing and transport automation systems [1].This Company has always been seeking to invest in research and development of high technology standards and through its many years of activity it has developed new types of products.
C.R.D. Centro Ricerche Ducati Trento (Italy - Rovereto) was founded in 2006 thanks to a cooperation between the University of Bologna, the University of Trento, and the Trento Province. It consists of a significant group of engineers dedicated to the development of innovative solutions for reduction of pollution and drive systems.
The proposed problem concerns the energy storage for railway signaling applications when a black-out occurs.

1.1.2 The problem

Ducati Energia is interested in the study of super capacitors UPS (Uninterruptible Power Supply) because of their numerous advantages:

- greater specific energy thanks to their composed element (graphene);
- scalability: number of capacitors proportional to autonomy required and cost proportional to number of capacitors;
- technology diffusion: used in the automotive as well as in the electrical fields;
- low maintenance: longer lasting if temperature controlled;
- faster to be produced compared to inertial batteries.

Moreover, in spite of a limited storable energy, super capacitors offer very high specific powers and very short charging times.
The analysed problem is the thermal characterisation of a novel energy storage system based on super capacitors. Super capacitor properties sensibly change as temperature changes and operation at high temperature (above a few tens of degrees Celsius) quickly leads to sub-optimal performance and even precocious failure.
In light of this consideration, there are two separate aspects to investigate. On one hand, the thermal behaviour of the core super capacitors must be characterised. Because of the relative novelty of super capacitor technology, the detailed behaviour of the devices as a function of temperature is not reported in the respective technical sheets. On the other hand, the cooling strategies to adopt when arrays of capacitors are arranged into standardised cabinets for UPS applications are to be studied. In this respect, one must pay particular attention to the dimensioning of the cooling infrastructure as well as to how the cooling power is distributed and delivered to the cabinets.

1.2 Electrothermal characterisation of the super capacitors

Since the super capacitors are relatively new products, both producers and customers do not have much information on their physical characteristics. Ducati Energia provided us with samples from two producers: Eaton Corporation Plc, a multinational power management company founded in the United States in 1911, and TIG Electronic Technology Co., Ltd., a newborn Chinese company established in 2001 in Shenzhen. Both Eaton's super capacitors from the XL60 product line and TIG's ones from the TIGSTOR family are rated 3000 F at 2.7 V.

Figure 1.1: Super capacitors

1.2.1 Heat capacity

In order to measure the heat capacity of the super capacitors we used two baths at known temperature. They were isolated from the surrounding environment with special containers.
One bath was kept at constant low temperature with a mix of ice and liquid water and was used to cool down the super capacitors at 0 °C. Once a super capacitor has been cooled, we transferred it to the second bath, which contained distilled water at room temperature. Finally, by measuring the temperature variation of the water in the second bath with a PT100 we could infer the heat capacity of the super capacitor. In fact, assuming that the heat exchanged by the capacitor Q_{SC} and by the water Q_{H_2O} are equal, we obtain:

$$C_{SC}\Delta T_{SC} = Q_{SC} \simeq Q_{H_2O} = c_{H_2O} M_{H_2O} \Delta T_{H_2O}, \tag{1.1}$$

where Q_{SC/H_2O} are heat, C_{SC} is the heat capacity of the super capacitors, $c_{H_2O} = 4181.3\,\mathrm{J/(kg\,K)}$ is the specific heat capacity of water, M_{H_2O} is the mass of the water in the room temperature bath, and ΔT are temperature variations.

$$C_{SC} \simeq \frac{c_{H_2O} M_{H_2O} \Delta T_{H_2O}}{\Delta T_{SC}}. \tag{1.2}$$

Table 1.1: Heat capacity and specific heat of the two models of super capacitors.

	EATON XL60	TIGSTOR
C_{SC} [J/K]	550 ± 30	460 ± 20
c_{SC} [J/(K kg)]	1110 ± 60	920 ± 50

1.2.2 Leakage current

Considering the fact that the super capacitors will be employed as batteries in a UPS, they will be for the most part of the time in a charged condition. Hence, the power consumed during such state is due to the leakage current at the operating voltage.
The simplest model of a real capacitor, shown in Figure 1.2, describes the leakage current as flowing past the ideal capacitor, through the parallel resistance R_P.

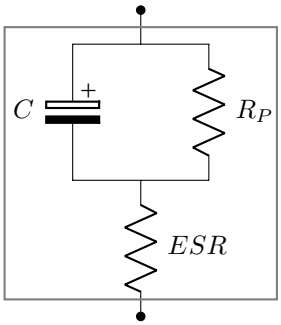

Figure 1.2: Simple model of a real (super)capacitor.

At full charge, the total resistance of a single capacitor is given by the sum of the parallel resistance R_P and Equivalent Series Resistance ESR:

$$R_{tot} = R_P + ESR \simeq R_P. \tag{1.3}$$

However, since $ESR \ll R_P$, we can neglect the contribution of ESR in the evaluation of the leakage current as:

$$I_{leakage} = \frac{V}{R_{tot}} \simeq \frac{V}{R_P}. \tag{1.4}$$

Eaton's XL60 rated values for operation at 2.7 V are:

$$ESR = 0.23\,\mathrm{m\Omega}, \qquad I_L = 5\,\mathrm{mA}, \qquad R_P = 540\,\Omega. \tag{1.5}$$

There are no rated values for TIGSTOR capacitors, but we assume they are similar to XL60 ones. Common values for R_P in standard capacitors range from MΩ to GΩ and thus the leakage current is much lower.

Direct measurement

Our first approach to the measurement of the leakage current has been a direct measure. An ammeter, in series with the super capacitor, measures the current passing through the circuit. The super capacitor is kept charged at 2.5 V, in an equilibrium state, by a voltage generator, and the effective voltage difference between the ends of the super capacitor is measured by a voltmeter in parallel. The complete circuit is shown in Figure 1.3.
We quickly observed that a tiny variation from the operating voltage 2.5 V, even of the order of mV, generated in the circuit currents even ten times larger than the expected leakage current, which is in the order of mA.
Moreover, the charge/discharge behaviour is modelled by an exponential, which reaches asymptotically the equilibrium state. This means that, given an initial distance from the equilibrium state, the system will need a time period longer than 4.5 time constants. The time constant of the exponential is $\tau = R_{Amm}C \simeq$ 3 h 20 min where $R_{Amm} = 4\,\Omega$ is the internal resistance of the ammeter and

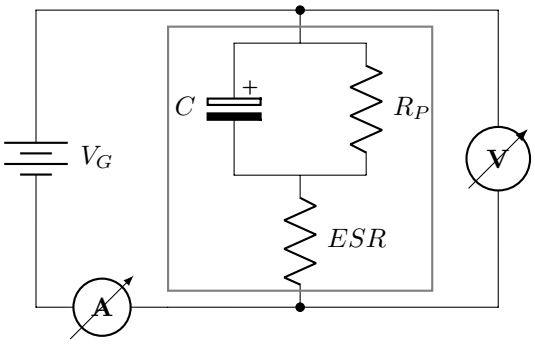

Figure 1.3: Circuit to measure the leakage current directly.

$C \simeq 3000\,\mathrm{F}$ is the super capacitor capacity. Hence we can understand how much time the circuit needs to reach equilibrium.
During our experiments we sampled a 15 h-long charge. The current flowing through the circuit had and initial value of 50 mA, while at the end of the measurement was 7 mA.
We fitted the data to an exponential function $I(t) = I_{leakage} + (I_{initial} - I_{leakage}) \cdot e^{-t/\tau_1}$, and obtained a value for the leakage current of $I_{leakage} \simeq 5.9\,\mathrm{mA}$. Figure 1.4 shows the curve obtained.

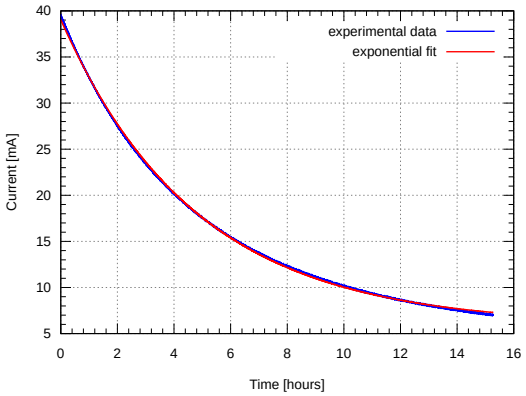

Figure 1.4: EATON XL60 15-hour long charge measure displaying the current flowing in the circuit versus time.

Since we know both the voltage at the end of the super capacitor and the leakage current, we can calculate the value of the parallel resistance R_P. Values are shown in Table 1.2.

Improvements A possible improvement to this measurement is to replace the ammeter with a known resistance, and measure the voltage at its ends with a voltmeter. Substituting the ammeter with a known resistance, smaller than the internal resistance of the ammeter, reduces the time constant τ_1 of the circuit and

Table 1.2: Due to the lenght of the measure, only a sample of the XL60 family has been tested.

	EATON XL60
I_L [mA]	5.9
R_P [Ω]	460

therefore allows for faster measurements. For example, using a 0.5 Ω resistance (adequately thermalised) reduces of eight times τ_1 and would allow to do the 15 h-long measurement in 2 h.

Self-discharge and constant current measurement

Another method we employed to measure the leakage current is to exploit the self discharge. The behaviour of the voltage at the ends of a capacitor is determined by the self discharge current flowing through the parallel resistance R_P, which is described by an exponentially decaying curve:

$$V(t) = V(t_0)e^{-\frac{t-t_0}{\tau}}, \tag{1.6}$$

where $\tau = R_P C$. Figures 1.5 (a) and (b) show the circuit used and the data obtained, respectively.
However, in order to measure R_P, we have to know the value of the capacity too. Hence, by charging the capacitor with a constant current and measured the variation of voltage at the ends of the capacitors, which is related to the capacity by:

$$C = I\frac{\Delta t}{\Delta V}. \tag{1.7}$$

Figures 1.5 (c) and (d) show the circuit used and the measurements plot of two super capacitors.
The resulting values for this method are shown in Table 1.3.

Table 1.3: Capacities have been obtained for a constant current charge of 5 min. The values of R_P have been obtained on a 120 min discharge.

	EATON XL60	TIGSTOR
C [F]	2550	2600
τ [h]	400	270
R_P [Ω]	565	370
I_L [mA]	4	7

From these data we can see that the capacity is comparable for the samples of the two manufacturers. The measure on EATON's super capacitor shows a lower leakage current I_L in comparison to TIG's one. It appears then that in the specific application for which they will be used, XL60 super capacitors would provide less power consumption. However we measured only two samples and therefore these values are not representative of the overall product quality.

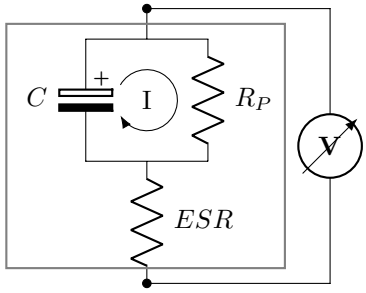

(a) Self-discharge measurement circuit

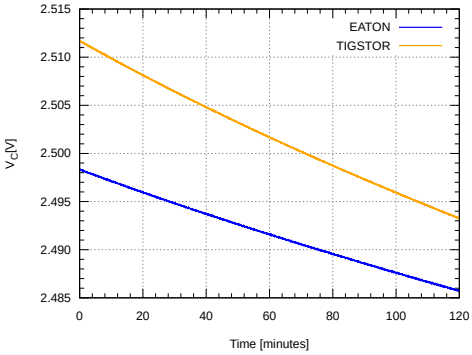

(b) Self-discharge measurement

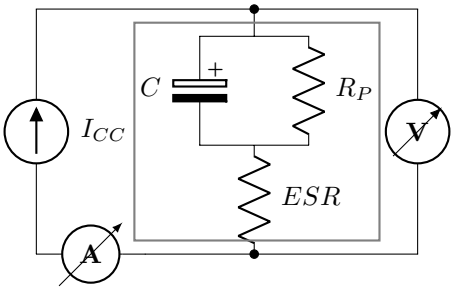

(c) Constant current measurement circuit

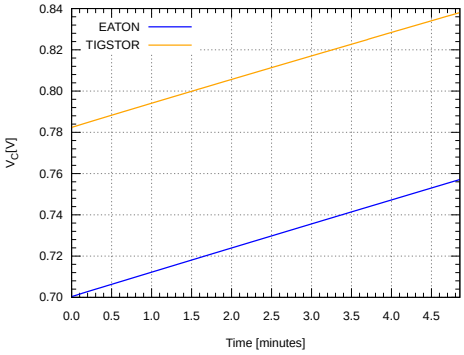

(d) Constant current charge measurement

Figure 1.5

Capacity depends on voltage From the self discharge data, we observed that the behaviour of the voltage cannot be modelled by a simple decaying exponential. In fact, by plotting $\log(V(t))$ as a function of time, one can see that the resulting curve is not a straight line as expected. Figure 1.6 shows such plot.

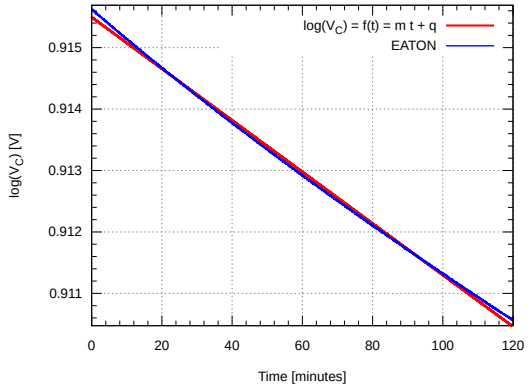

Figure 1.6: Logarithmic plot of the voltage as a function of time, during the self-discharge.

This means that τ is not constant in time and, therefore, that either one or both the capacity and the parallel resistance R_P have a voltage dependence.
Hence, it is very important to use the same operating conditions in each test on the different samples. Otherwise, the estimations of the physical characteristics cannot be compared.

Proposed procedure

In order to carry out the measurement most efficiently, we propose a method to measure a few characteristics of a single capacitor.

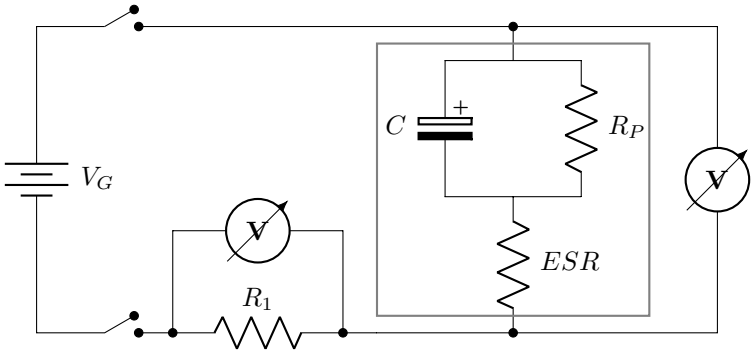

Figure 1.7: Circuit for the proposed measurement procedure

The procedure, starting with a non charged capacitor, is composed of three main parts:

1. Charge with constant current until 2V [40 min, with 2 A]

2. Direct measurement of leakage current at working voltage 2.5 V [2 h]
3. Self discharge [2 h]

Specifically, the parts are defined as follows:

1. The first part allows the evaluation of C by using Equation 1.7 with a linear fit. Considering a constant supplied current of 2 A, around 40 min are needed in order to charge the capacitors up to 2 V.

2. In the second part, the capacitor is supplied with a voltage source set at 2.5 V and the voltage at the ends of the resistance $R_1 \simeq 0.5\,\Omega$ is measured. Using the Ohm law $I = V/R$ we can obtain $I(t)$ and from an exponential fit

$$I(t) = I_{leakage} + (I_{initial} - I_{leakage}) \cdot e^{-t/\tau_1} \tag{1.8}$$

we can extract an estimation for $I_{leakage}$.

3. In the third part, the super capacitor is disconnected from the rest of the circuit and the voltage at its ends is measured. Collecting the data and using Equation 1.6 to fit them, leads to the evaluation of $\tau = R_P C$. Finally, from the value of C obtained from the first part of the measurement one can derive the value of R_P, and thus of $I_{leakage} = \frac{2.5\,\mathrm{V}}{R_P}$.

1.2.3 Lifetime and operating temperature

Producers warn their clients that the estimated lifetime of the super capacitors for a certain applied voltage is valid only at the operating temperature specified in the datasheet. In fact, the lifetime is expected to degrade for higher applied voltages and for higher operating temperatures.
For this reason, usually lifetime is evaluated with accelerated ageing, which wears the capacitors out in a shorter time than at standard conditions. In order to minimize the time required for such testing, capacitors are often tested at the maximum working temperature and voltage.
As a rule of thumb, electrochemical double layer capacitor (EDLC) lifetime at a given voltage halves every 10 °C increase in temperature.

$$L_x = L_0\, 2^{\frac{T_0 - T_x}{10}} \tag{1.9}$$

Since the expected lifetime of EATON XL60 is a bit more than 10 years at 2.7 V and 25 °C, the estimated lifetime at 65 °C is 16 times shorter. The period required for wearing out such super capacitor in the worse conditions is still approximately 5000 h (7-8 months).
Unfortunately, we had less than a week to complete the experiments, therefore we could not afford to do analogous measurements. Moreover, tests at very high temperature could become dangerous, both for the instrumentation and the people operating it. In fact, much smaller capacitors can produce discrete explosions, if supplied with reverse polarised voltage and/or incorrectly handled. Hence, given

the amount of energy a super capacitor can store, it is not wrong to suppose that it could exhibit a dangerous behaviour if operated at too high temperatures.

1.3 Parametric dimensioning of the cooling system

In order to cool the equipment that will make up the UPS system, we had to quantify the thermal dissipation of the equipment itself in the various operating statuses. The total thermal power dissipated per cabinet has then been used as an input to model the thermal insulation system of the cabinets themselves. Finally, we used publicly available climate data to estimate the energetic costs of the cooling system over an average year.

1.3.1 Thermal output of the equipment

Table 1.4: Typical thermal dissipation power of the different components of the UPS, grouped by module and by cabinet type. Where a question mark is present, the value of the typical dissipation is guessed; where marked N/A, the typical dissipation is not known. The suffix -R indicates resistors.

Component	#	Peak power (W)	Typical power (W)
Single module			
BMS	1	3	1.5
SUPERCAP	18	0.33	0
BALANCE-R	18	0.76	0.35?
DISCHARGE-R	1	1114.8	45?
CHARGE-R	1	25	N/A
STATIC-INT	1	9.5	0
Control cabinet			
AC/DC-30	1	210	N/A
AC/DC-300	1	210	N/A
DC/DC-48	2	31.1	N/A
DC/DC-24	2	31.1	31.1
SU-300x8	1	1320	N/A
HMI-cRiO-9030	1	40	3.4
HMI-LCD	1	35	5
SuperCap cabinet			
HMI-REM-11180	1	13.7	2.5
HMI-REM-11120	1	1.76	1.05
HMI-REM-11154	1	1.2	0.96
HMI-REM-11178	1	2	0.8
MODULE	12-18	1	N/A

In order to quantify the thermal output of the equipment in each cabinet, we compiled a table of the power dissipated as heat by each device. The table,

organised by cabinet type (namely: single module, control cabinet and SuperCap cabinet), lists for each device its peak and typical power dissipated and the number of each component present in the cabinet. An example of this table is shown in Table 1.4. Subsequently, for each operating state, we evaluated the power dissipated by each component, listed as a fraction of the peak power consumption. The value of the power dissipated as heat for for some components in some operating states was not known, and was therefore guessed. For instance, we conservatively estimated that the balance resistor (BALANCE-R of Tab. 1.4) of each super capacitor on average dissipates half of its peak power, and that the maintenance discharge resistor (DISCHARGE-R), on average only dissipates 4% of its peak power over the 30 minutes of a single module discharge cycle.
Regarding the estimates of total thermal dissipation in
Simple accounting (see Section 1.6.1 for the description of the computer program used) allows us to compute the estimated total thermal power dissipated by each module and cabinet. The results are reported in Table 1.5. Tab. 1.5, two comments are due. First, the powers at play are generally low, especially for the stand-by state (STATE 1), the one in which the system will be for most of its lifespan. Second, the peak power of approximately 1.5 kW is attained in the control cabinet and it is a figure that represents peak dissipation in the event of a black-out (STATE 6), which is expected to only last a few minutes. It hence does not involve heating of the super capacitors, which are physically separated in dedicated cabinets.

Table 1.5: Power dissipated by a single module and by different cabinet types for each of the different operating states.

	state - power dissipated (W)					
COMPONENT	1	2	3	4	5	6
(time)		30'	30'	16-24h	<4h	10'
MODULE	8.34	12.2	46.1	26.5	1.5	12.2
CONTROL CABINET	212	764	380	380	380	1490
SUPERCAP CABINET	169	238	207	187	46.6	238

1.3.2 Insulation, geometry and cooling requirements

The modular design Ducati Energia proposes consists of 7 standard-size cabinets, with the plan to add a thermal insulation layer inside each cabinet.
In order to model the heat flow between the inside and the outside of the cabinet, we leverage on a well known formal equivalence between thermal and electrical conduction, depicted in Fig. 1.8-(left). Indeed, the heat flow $P = \dot{Q}$ through several layers of materials sandwiched between two thermal baths at temperatures T_1 and T_2 is akin to the electrical current flowing through a series of resistors kept at potential V_1 and V_2 at either side. In the same way, the thermal inertia of an object (i.e., its heat capacity), is equivalent to inserting a condenser (i.e., an electrical capacity) in the equivalent circuit. In the case of a cabinet, in

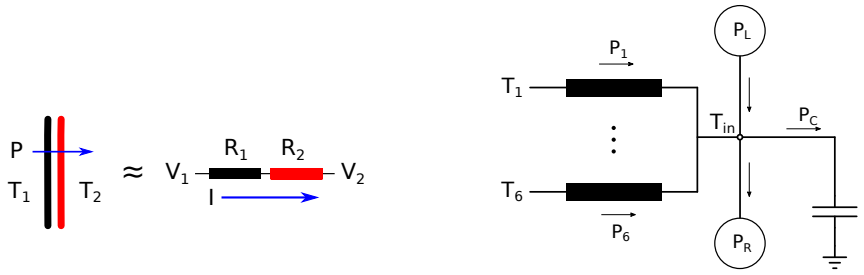

Figure 1.8: (Left) Equivalence between thermal and electric conduction. (Right) Electric equivalent circuit for a cabinet with six walls, each of which can be in contact with a thermal bath at a different temperature.

which each face can be in contact with a thermal bath at a different temperature, the equivalent circuit features the total resistance corresponding to each face connected in parallel to the other faces. Finally, the power dissipated by the load and the power removed by the cooling system can be seen as current generators, leading to the equivalent schematic in Fig. 1.8-(right).
The equivalent circuit is described by the differential equation:

$$C\frac{dT_{\text{in}}}{dt} = \sum_{i\in\text{faces}} \frac{T_i - T_{\text{in}}}{R_i} + P_L - P_R, \tag{1.10}$$

where C is the total heat capacity of the cabinet, R_i is total thermal resistance of the i-th face of the cabinet, T_i is the temperature outside the i-th face, T_{in} is the internal temperature and $P_{L,R}$ are, respectively, the load and refrigeration powers. This simple model assumes that the temperature is uniform inside the the cabinet, and that both load and refrigeration powers are homogeneously applied throughout the internal volume.
The thermal resistance of the faces of the cabinet was computed based on the surface area of the face itself, and on the physical characteristics of cabinet wall and insulation material, according to the relation:

$$R = \frac{\sigma_{\text{air}}^{-1} + \sum_i d_i\sigma_i^{-1}}{A}, \tag{1.11}$$

where A is the surface area of the face, σ_{air} is the heat conductance of the air film on the inside of the cabinet wall and d_i and σ_i are the thickness and heat conductance of the i-th layer that the cabinet wall is made of. In our model, we assumed that the cabinet wall is made of one layer of 1.5 mm steel [$\sigma_{\text{steel}} = 300\,\text{W}/(\text{m K})$] and one layer of aerogel as the insulating material [$\sigma_{\text{aerogel}} = 0.014\,\text{W}/(\text{m K})$]. The thickness of the insulation is left as a parameter to be optimised.
For the modelling of the heat capacity of the inside of the cabinet, we used the known heat capacity of the super capacitors as found experimentally in Sec. 1.2.1 and assumed that the whole covolume is filled with air (heat capacity per unit volume $= 1205\,\text{J}/(\text{m}^3\,\text{K})$). Since the effect of a large heat capacity is to limit the

increase of the temperature in the absence of active cooling, whenever we had not got available the values of the heat capacity for other components, we simply assumed an equivalent volume of air.
Equation 1.10 can be easily integrated numerically to obtain the full dynamical evolution of the temperature inside a cabinet as a function of time, thermal load, cooling power and outside conditions (Section 1.6.2).

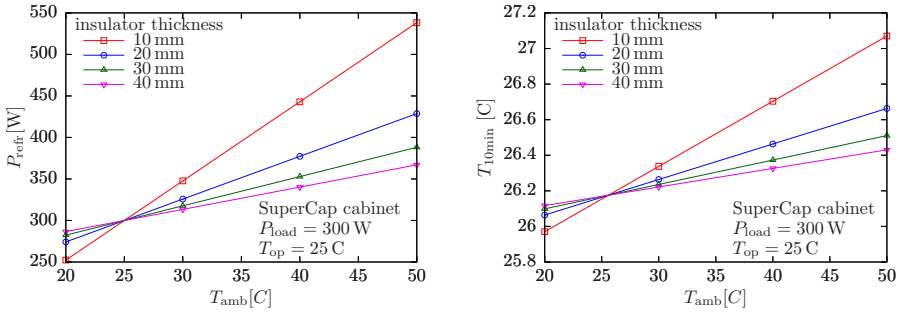

Figure 1.9: Single cabinet refrigeration power P_R needed to maintain an operating temperature of $T_{\text{op}} = 25\,°\text{C}$ (left) and internal temperature starting from $T_{\text{op}} = 25\,°\text{C}$ after 10 minutes without cooling $T_{10\text{min}}$ (right), both as functions of the external temperature (equal for each wall of the cabinet) and insulation thickness.

A first question to answer is the nature of the thermal insulation: should one thermally insulate the cabinet? As already noted, the super capacitors are sensitive to high temperatures, which quickly degrade their physical properties and shorten their lifespan. For this reason, we concentrated on the most extreme temperatures that we envisage could be reached once the UPS system is deployed. The standard test case we considered is an external temperature of $T_{\text{amb}} = 50\,°\text{C}$ and an operating temperature that should be kept constant at $T_{\text{op}} = 25\,°\text{C}$. In Fig. 1.9-(left) we show the cooling power needed to maintain a SuperCap cabinet with a thermal load of 300 W stationary at 25 °C for different thicknesses of the insulation layer and different ambient temperatures. As expected, less power is needed to keep the cabinet cool in hot weather if the insulation layer is thickened. However, since the heat entering the cabinet is inversely proportional to the insulation thickness, one find that the gains of adding more insulation are not very significant over 30 mm of aerogel. For instance, at $T_{\text{amb}} = 50\,°\text{C}$, going from one to two centimetres of aerogel saves approximately 115 W, but adding an extra centimetre of aerogel on top of that only saves an additional 41 W.
In the event of a black-out, with the UPS in operating state 6, we expect that the refrigeration system will also stop working. In this situation, it is important to make sure that the temperature inside the cabinets does not increase beyond what is safe for the super capacitors. We assumed that the black-out lasts for 10 minutes and we computed the final temperature $T_{10\text{min}}$ of a cabinet that was initially kept at $T_{\text{op}} = 25\,°\text{C}$ with a thermal load of 300 W. We plot in Fig. 1.9-(right) $T_{10\text{min}}$ for different external temperatures and different insulation thicknesses. Even for the highest external temperature of $T_{\text{amb}} = 50\,°\text{C}$, we see

that there is no real need to have more than 20 mm of aerogel; in this case, the cabinet temperature would increase over T_{op} by less than 2 °C.
The control cabinet, being less sensitive to high temperatures, requires a separate discussion. Indeed, in light of the fact that the equipment in the control cabinet can resist temperatures of up to 70 °C, we noted that it is not convenient to use thermal insulation at all, and rather set up some form of permanent passive cooling. In fact, without insulation, during stand-by operation the internal temperature is always just a few degrees above the ambient temperature. In the worst case scenario of a black-out, with the equipment inside the control cabinet dissipating approximately 1.5 kW, and assuming $T_{\text{amb}} = 50\,°\text{C}$, $T_{10\text{min}}$ remains below approximately 65 °C.
We conclude that 20 or 30mm of aerogel insulation should be considered for the super capacitor cabinets, while the control cabinet should rather be kept not insulated and left free to exchange heat with the surroundings. It is also advisable to avoid thermal contact between the control cabinet and the other cabinets, and to arrange the cabinets with fewer super capacitor modules (hence dissipating less heat) to the sides of the array, so as to shield the cabinets with more modules from potentially higher external temperatures.

1.3.3 Dependence on local climate

It was already underlined in the previous section how both the dimensioning of the cooling system and the thermal insulation strategy will crucially depend on the local climate of the area where the UPS system will be deployed.
We used publicly available local weather statistics to estimate the total cooling energy needed (see Section 1.6.3). The system is expected to stay in stand-by operation for most of the time, so that only that operating state is considered. Furthermore, we assumed that whenever the ambient temperature is such that $T_{\text{amb}} \leq T_{\text{op}} - \Delta T$ ($\Delta T = 5\,°\text{C}$ in the following results), some form of passive cooling is used and the active refrigeration is kept off.
As an example of this calculation, for 20 mm aerogel insulated cabinets operating at $T_{\text{op}} = 25\,°\text{C}$, we envisage the yearly energy consumption to be approximately 3000 kWh in Palermo, 1700 kWh in Venice and 300 kWh in Tarvisio. Of course, these are estimates of the energy that needs to be subtracted from the cabinets to keep them cool, and they must be corrected for the efficiency of the cooling apparatus used, for which we had no data available.
Using this calculation strategy, by changing the characteristics of the UPS thermal model (most notably the insulation), one can hope to further optimise the thermal properties of the system and minimise its total cost of ownership.
In conclusion of the present section, a word of caution should be used since we did not have time to carefully estimate the errors introduced in different steps of the modelling. As a rule of thumb, we can guess that the estimates provided throughout this section be precise to approximately 15%, making clear that we did not assess this figure in any scientific way, but rather based on experience and intuition.

1.4 Air conditioning distribution strategy

1.4.1 CFD simulation

Introduction

We decided to perform some CFD simulation in order to find out an efficient geometry for the cooling system of the super capacitors cabinets. We focused on a dry-air cooling system, since it could help in avoiding dew formation, by both reducing the air humidity in the cabinet (a closed-loop cooling system could be used to this purpose) and avoiding the presence of cold surfaces (the pipes which constitute air inlets could be eventually insulated if turned out to be critical).

Brief description of the simulation

The super-capacitor modules are insulated from the external environment through an outer metallic box (with thickness $\sim 2\,\text{mm}$), coated on its inner sides with a thermally insulating material (aerogel, with thickness$\sim 20\,\text{mm}$). We reasonably assumed the outer face of the metallic box to be at the environment temperature, which was fixed at $T_{amb} = 50\,^{\circ}\text{C}$.
We assumed a velocity of the air at the inlets $u_0 = 0.5\,\text{m/s}$, which we considered to be a reasonable order of magnitude estimation. A typical length scale is set by the space between the cabinets, $L \sim 10\,\text{cm}$. This gives a Reynolds number $R = \frac{u_0 L}{\nu} \simeq 2800 \gg 1$, so the turbulence needs to be taken into account. The temperature of the air at the inlets was assumed to be fixed at $T_0 = 22\,^{\circ}\text{C}$. (One can then play with these initial values, namely u_0 and T_0, and with the geometry of the system in order to obtain better results).
It is apparent that lots of physics is involved here (thermal conduction, heat fluxes from the SuperCap modules, non-isothermal turbulent airflows, ...); we thus decided to perform a simpler and quicker 2D simulation instead of the 3D one, whose computational cost is evidently much higher. We considered the section of the cabinet cutting it from front to back. The modules were modeled as simple rectangles whose upper face exchanges heat with the cabinet. This choice is motivated by the fact that the upper face is covered with an alluminium plate characterized by a larger thermal conductivity than the other faces of the module that are made in plastic. We decided to look at the most improbable and unfavorable case in which each module is heating.

Geometry choice

We first of all performed some even simpler simulations (in which only the airflows are simulated, without any heat transfer among the different parts of the system) to decide the geometry of the air conditioning system. We first of all tried a single-inlet geometry, but it is apparent from Fig. 1.10.a that the air flux on top of the modules is not optimal, which we think will make such a cooling geometry quite inefficient.
The airflows may however be redistributed on top of each module to take away the heat they generate most efficiently, as shown in Fig. 1.10.b. We expect

that directly "blowing" onto the aluminum dissipative plates can keep the super capacitors under the proper temperature conditions.

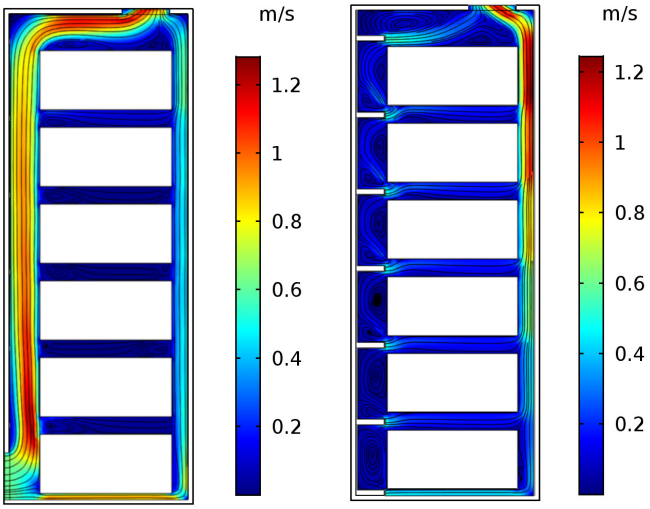

(a) Single-inlet system **(b)** Multiple-inlets system

Figure 1.10: Air cooling systems

Full simulations

We then performed the full simulation with this second geometry, which seems more promising in terms of efficiency. The results for the velocity field and the temperature field are plotted in Fig. 1.11.a and 1.11.b respectively.
It can be seen that the 20 mm aerogel layer is quite effective in thermally insulating the cabinet[1]. This may suggest that 3D simulations may be performed by simply neglecting the outer environment with little error. This could help a great deal in speeding up an otherwise extremely resource-demanding simulation.

1.5 Recommendations and conclusions

We measure that the capacity of a super capacitor is not linear with tension, so the treatment of this system needs non-standard methods. By analysing the operation of the UPS we found that the electronic cabinet is the biggest source of heat so we suggest to put it far away from capacitors cabinets.
Energy balance calculations allow us to say that the electronic cabinet does not need refrigeration, but just active air cooling. In this case we assumed the environment as a thermal bath at 50 °C. Energy balance calculations also show

[1]Recall moreover that the simulations refer to the extreme case of $T_{amb} = 50\,^{\circ}\mathrm{C}$

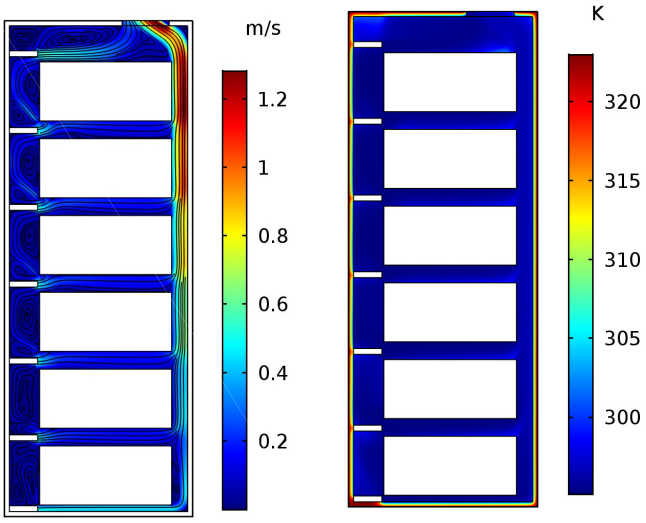

(a) Velocity field **(b)** Temperature field

Figure 1.11

that in case of discharge of the whole system (and in case of capacitors recharge) the temperature increases less than 2 °C for a 20mm aerogel layer (Fig. 1.9). Lastly, we found that one air duct which insert cooled air in each cabinet does not efficiently cool down the capacitors. We propose instead a more efficient geometry which inserts cooled air directly into each capacitor module, by directing the air flux with smaller air ducts.

Bibliography

[1] `https://www.ducatienergia.com`

[2] `http://www.eaton.com` and `http://www.cooperindustries.com/content/public/en/bussmann/electronics/products/eaton-supercapacitors/cylindrical1/xl-series.html`

[3] `http://www.tig-energy.com`

1.6 Technical description of the programs

1.6.1 Accounting of thermal dissipation: `power.py`

Author and rights owner Jacopo Nespolo

Type Python script.

Dependency Python runtime, Numpy numerical library.

Input Table of per component and per operating state thermal dissipation.

Output Total per module/cabinet and per operating state thermal dissipation.

The program `power.py` is a Python script with no external dependencies. It takes as input a plain text, space separated table with 10 columns. The table is divided into three stanzas (`#control electronics cabinet`, `#SuperCap cabinet` and `#modules`). The values of the columns are as follows:

0. Component identifier
1. Number of the current component in the current group
2. Peak power consumption
3. Typical power consumption (not used in calculations, can be `N/A`)

4–9 Respectively, operating states 1 through 6.

`power.py` parses the table and computes, for each state, the total power dissipated by a single module, the control cabinet, or a single 18-module cabinet.

1.6.2 Dynamics of cabinet temperature: `libthermocabinet.py`, `thermocabinet.py`, `thermocabinet_full.py`

Authors and rights owners Jacopo Nespolo and Alberto Nardin (`libthermocabinet.py`), Jacopo Nespolo (`thermocabinet*.py`)

Type Python script.

Dependency Python runtime, Numpy numerical library.

Input Insulator thickness, thermal load, cooling power, ambient temperature, target internal temperature, number of SuperCap modules inside, heat capacity offset.

Output Cooling power required to reach taget temperature (as offset from the one provided as input), stationary temperature, temperature after 10 minutes without cooling.

The programs `libthermocabinet.py`, `thermocabinet.py` and `thermocabinet_full.py` numerically integrate the differential equation describing the time evolution of the temperature inside the cabinet or solve the algebraic equation to obtain the stationary conditions thereof.
`libthermocabinet.py` is a simple object oriented library that provides an abstraction layer for the description of cabinets. Cabinet objects are implemented as a collection of surface objects, each of which can be independently tuned with different cabin wall thickness, insulating thickness, insulatiion and build material (and hence different thermal properties) as well as different boundary conditions, i.e., external temperatures. The physical computations (thermal resistances of surfaces and complete cabinets, temperature dynamics given boundary conditions, etc.) are also implemented here.
`thermocabinet.py` depends on `libthermocabinet.py` and deals with the problem of a single cabinet at a time. It features a versatile command line interface for ease of use and scriptability:

```
$ ./thermocabinet.py -h
usage: thermocabinet.py [-h] [-i INSULATION_THICKNESS] [-L THERMAL_LOAD]
                        [-R COOLING_POWER] [-T AMBIENT_TEMPERATURE]
                        [-N NMODULES] [-C HEATCAP_OFFSET] [--Ttarget TTARGET]
                        [--plot]

optional arguments:
  -h, --help            show this help message and exit
  -i INSULATION_THICKNESS, --insulation-thickness INSULATION_THICKNESS
  -L THERMAL_LOAD, --thermal-load THERMAL_LOAD
  -R COOLING_POWER, --cooling-power COOLING_POWER
  -T AMBIENT_TEMPERATURE, --ambient-temperature AMBIENT_TEMPERATURE
  -N NMODULES, --Nmodules NMODULES
  -C HEATCAP_OFFSET, --heatcap_offset HEATCAP_OFFSET
  --Ttarget TTARGET
  --plot
```

It prints to standard output a single line of space separated values, thus allowing its output to be piped to other programs or parsed easily. The values are (in order): thermal load, target temperature, ambient temperature, insulation thickness, cabinet heat capacity, cooling power to maintain the target temperature, stationary temperature with the cooling power provided in input, temperature after 10 minutes without cooling starting from the target temperature. Note that, for the control cabinet, it may be more significant to compute the $T_{10\mathrm{min}}$ starting from the stationary temperature instead of the target temperature: this is easily achieved by changing a single line of code and can be automated in the code by adding an extra input flag.
`thermocabinet_full.py` also depends on `libthermocabinet.py` and is a preliminary code, with hardcoded parameters. For each operating state, it computes the total cooling power needed to keep cool the whole UPS system, comprising one control cabinet without thermal insulation and without active cooling and 6 SuperCap cabinets (4 with 18 modules and 2 with 12 modules).

It further provides the stationary temperature of the control cabinet in each operating state.
Despite having its parameters hardcoded, its internal working is modular and can be used as a solid base to build a fully interactive program. Indeed, it is a dependency of `yearly_energy.py`, detailed in the next section.

1.6.3 Energy expenditure: `yearly_energy.py`

Author and rights owner Jacopo Nespolo

Type Python script.

Dependency
Python runtime, Numpy numerical library, `thermocabinet_full.py` and dependencies thereof.

Input Statistical weather file (`*.stat`, as provided by EnergyPlus).

Output Yearly cooling energy in KWh.

The program `yearly_energy.py` internally uses the routines of `thermocabinet_full.py` to estimate the cooling power needed to keep the super capacitor cabinets in the stand-by state at operating temperature given the value of the ambient temperature. It integrates this value over the hourly average temperatures provided by the climate data file ("Average Hourly Statistics for Dry Bulb temperatures" in EnergyPlus' records) to compute the total cooling energy needed over the timespan of a year. One assumption the program makes is that some form of passive cooling is used as long as the ambient temperature is lower than the operating temperature minus 5 °C, i.e., whenever $T_{\text{amb}} \leq 20\,^{\circ}\text{C}$ if $T_{\text{op}} = 25\,^{\circ}\text{C}$.
For convenience, the program internally parses the climate data file, so that no editing of the file is needed on the user's side.
The parameters of the UPS (thermal load, insulation, etc.) are hardcoded; it is however easy to implement a full command line interface to allow the user to interactively change them.

1.6.4 Data Acquisition Scripts

Author and rights owner Davide Bazzanella and Riccardo Franchi

Type IPython script in (Jupyter notebook).

Dependency IPython runtime, Numpy numerical library, Pandas library, matplotlib library, usbtmc library

Devices multiple Agilent 34410A multimeters connected through USB

Output Data acquisition in `csv` and `pickle` file formats

These scripts have been written to control a number of Agilent 34410A multimeters and to complete specific measurements. Therefore, they require the modification of inner parameters in order to carry out other tasks, e.g different instrumentation or measurements. This is an important feature because it allows the modification of the control procedure while running. They can be used as a template for future measurements. The scripts retrieve from the instruments the acquired data and save it to `csv` and `pickle` files.

CHAPTER

TWO

DYNAMICAL STABILIZATION OF A CABIN ENTERING THE SNOWSTATION

I. Amelio, M. Di Giovanni, M. Endrizzi, S. Huber, D. Scappini, A. Saha and R. Haghani

2.1 Introduction

This work concerns the detailed analysis of the dynamics of a cable-hauled detachable gondola lift manufactured by LEITNER Ropeways company.
In particular, during the IPSP 2018 week, our team widely investigated the crucial moment when the cabin enters in the station undergoing a strong deceleration. This determines an oscillatory motion of the cabin that decreases the passengers safety and comfort, while increases the risk of mechanical components damage. So, the main task proposed by the company was to stabilize the cabin motion, trying to damp the oscillations as much as possible.
It is interesting to observe that the physical principle underlying the problem falls in the class of "shortcuts to adiabaticity". With this we mean that stabilization is intrinsically dynamical, and time evolution is far away from being adiabatic, where here the adiabatic limit would correspond to very slow accelerations, so to keep at any time the cabin axis vertical. We mention that the analogue quantum problem is of research interest in the community of quantum control and optimization: here a trap has to be moved with the least possible excitation of the wavefunction of the trap particle [Sorensen2016].
Initially, we report the company demands starting from the presentation of LEITNER Ropeways and, subsequently, describing the gondola lift structure in order to explain clearly the problem and how we faced it. Then, the second section is dedicated to the mathematical model of the system, focusing the attention on the equation of motions and on the action of the tires which decelerate the cabin. Finally, the analysis of the results and the conclusions are illustrated, giving also some tips to further develop the proposed solutions.

2.2 The task

2.2.1 The company

LEITNER Ropeways is a division of the High Technology Industries (HTI) Group, an umbrella organization that comprises other important brands such as POMA (cable-hauled transportation systems), AGUDIO (material ropeways), MINIMETRO (rope-hauled vehicles), PRINOTH (snow groomers and tracked utility vehicles), DEMACLENKO (snow-making systems) and LEITWIND (wind turbines).

LEITNER Ropeways, together with PRINOTH and DEMACLENKO companies, makes HTI Group the world's first single-source supplier for winter sport technologies.

In particular, the South Tyrol company LEITNER Ropeways has been producing cable-hauled transport systems since 1888. The constant research of high-tech solutions and innovative designs has led the company to be the world's leading manufacturers of detachable gondolas and chair lifts as well as aerial tramways, funiculars, inclined elevators and fixed grip ski lifts.

The great effort dedicated to research and technological development always focuses particularly on passenger comfort and, even more, safety. This leads the company to be at frontier of technical innovation, by setting the example for other manufacturers.

2.2.2 Rope-hauled detachable gondola lift

Detachable gondola lifts are monocable systems in which the vehicles are detached from the haul cable in the stations.

Initially, the haul rope carries the gondola lift to the station entrance with constant velocity. At this point, a mechanism detaches the lift from the cable so that the trolley at the top end of the cabin can continue its route leaning on a rail (element ① Fig. 2.1-(left)). Meanwhile, a tip located under the gondola lift runs through a guide in order to avoid oscillations along the transversal direction during its path inside the station (element ③ Fig. 2.1-(left)).

The gondola lift deceleration is due to a train of 37 tires (with a diameter equal to 0.5 m) situated above the rail on which the trolley runs (Fig. 2.1-(right)). A synchronization mechanism gives to the first tires a tangential velocity equal to the one of the entering cabin which is 6 m/s. A system of belts and pulleys with different radii gives to the other tires distinct angular velocities and, moreover, these are in contact with a plate fixed over the trolley (element ② Fig. 2.1-(left)) in such a way that they exert a "friction" force which decelerates the whole system

to a final velocity equal to 0.27 m/s.

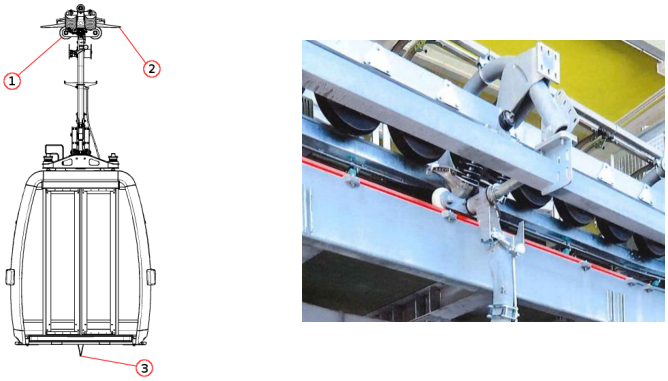

Figure 2.1: (Left) Scheme of the cabin under study where one can see highlighted the components helpful to understand the system dynamics. (Right) Zoom of the tires acting on the plate carried by the trolley.

The description of this friction force is a topic that will be addressed later in the present chapter; however, one can expect that the friction will depend on the difference among the plate velocity and the one of the tires. Then, according to the different ratios between the radii of the tires, one can set a certain profile of the angular velocities as function of the position along the path and therefore control the acceleration/deceleration of the cabin in order to slow down/speed up it to the desired velocities.
Subsequently, the gondola lift maintains a constant velocity following a circular path during which the people can get off and on the cabin. Finally, other 37 tires accelerate the gondola lift to the velocity of 6 m/s and then it leaves the station.

2.2.3 The problem

LEITNER Ropeways has always studied innovative solutions to take care of the passenger safety and comfort. In fact, a collaboration with a German university allowed the company to obtain a software able to solve the dynamics of the cable-hauled detachable gondola lift when it enters/leaves the station. Using this tool, Leitner's engineers can find various configurations of the tires velocity which determine a smoother cabin motion with small oscillations.
This software offers the chance to modify many parameters concerning the gondola lift dynamics, e.g. mass and initial velocity of the cabin, length of the arm connecting the trolley to the cabin, tires velocity, etc. However, LEITNER Ropeways wants to improve the performance of the gondola lift acceleration/deceleration process introducing a new variable: the inclination of the station. Unfortunately, the software structure does not allow to modify the code in order to add the inclination angle.
So, the first request of the company was to analyze the system dynamics

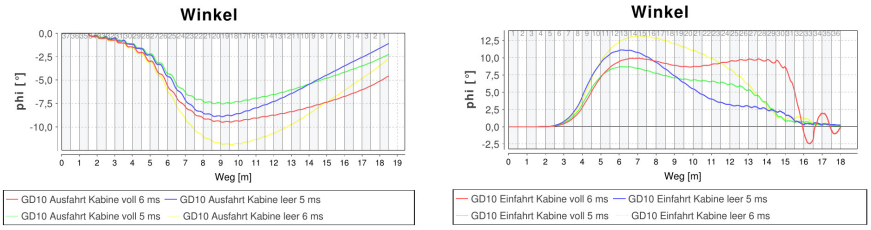

Figure 2.2: These plots illustrate some results considering different conditions where the mass carried by the cabin and its initial velocity change. (Left) The plot shows the oscillation angle as function of the position while the cabin is leaving the station. (Right) The plot presents the oscillation angle as function of the position during the cabin entry.

considering this new parameter α (among 0 and $\sim 7\,^\circ$) and, subsequently, to develop a new program, editable and with a user-friendly GUI, able to simulate the cabin motion. In particular, the program should be implemented in such a way that, with a little bit of effort, one could manage to obtain a tires velocity configuration which guarantees a smooth cabin motion given a certain initial condition.
Moreover, the second demand was to investigate if the inclination could bring some benefits to the acceleration/deceleration process, reducing the length needed to accelerate/decelerate the cabin, the oscillation amplitude of the cabin and the force provided by the tires to accelerate/decelerate the gondola lift.

2.2.4 Approach to the problem

In order to meet the company's demands, the most important step to face up is to find the equations of motion describing the system dynamics. So, initially, we divided our team in two groups to try different mathematical models and approaches. We then decided to model the gondola lift as a physical pendulum attached to a point-like mass describing the trolley, and to adopt the Lagrange formulation to look at the equations.
Subsequently, we developed the code to numerically solve the two differential equations obtained analytically. In this way, we had a useful tool to verify the correctness of the equations and to investigate the right description of the force due to the tires action on the trolley which, indeed, was the second important aspect of our problem. We considered two possible descriptions, taking also into account some results we found in the literature.
Finally, we added an easy GUI to the code and we tested its practicality and utility by studying the system dynamics in different conditions with the purpose to improve the performance of the gondola lift acceleration/deceleration mechanism.

2.3 Modeling the dynamics

In this Section we go through the derivation of the equations of motion, considering first the mathematical model of the system trolley-gondola and, subsequently, the forces involved. Particular emphasis is given to the description of the tires action since this determines strongly the oscillatory behavior of the cabin.

2.3.1 Minimal description/sliding pendulum model

The first question to be asked concerns which elements of the real device need to enter the mathematical model in order to capture the essential physics of the acceleration/deceleration of the gondola and stabilization of its oscillations. Leitner previous experience shows that a model with two degrees of freedom, one for the trolley position running on a straight line and one for the angle of the gondola center of mass, behaves satifactorily. The distance trolley-gondola is fixed, and we will refer to this model as the *sliding pendulum*.

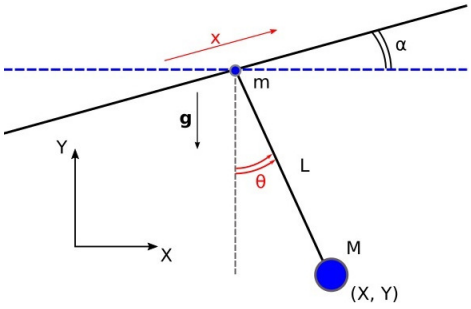

Figure 2.3: Scheme of the mathematical model of the system.

On the other hand, just the angle degree of freedom, with the dynamics of the trolley constrained to move with a fixed velocity in any point of its trajectory, describes a completely different dynamics; this it has been checked also by ourselves and will be presented at the beginning of the Analysis of the Dynamics section (2.4.1).
The sliding pendulum model is depicted in Fig. (2.3), where x indicates the one-dimensional trolley coordinate, α the inclination of the trolley-gondola segment with respect to the vertical axis (defined by gravity force $\vec{g}$), and (X, Y) is the position of the gondola center of mass in the vertical plane. We remark that the pendulum length L is an effective quantity chosen so that ML^2 equals the moment of inertia of the cabin around the pivot.
The trolley and gondola have masses m and M respectively, with real values of the order of $m \simeq 125$ kg and $M \simeq 1700 - 2400$ kg. The mass of the gondola lies in a broad range due to the variable number of passengers. We can also consider a friction (or viscous) angular force $F_\theta^{fr} = -\text{sign}(\dot{\theta})\Gamma_0$ (or $F_\theta^{visc} = -\gamma\dot{\theta}$), while the action of the control wheels on the trolley will be modeled later as an external force $F_x(x, \dot{x})$.

2.3.2 Equations of motion

Since the system presents two constraints, the trolley 1D guide and the trolley-gondola distance L, it is convenient to work with the Lagrange formalism. The Lagrangian with no L constraint and no external drive is

$$\mathcal{L}(x,\dot{x},X,\dot{X},Y,\dot{Y}) = \frac{m}{2}\dot{x}^2 + \frac{M}{2}\left(\dot{X}^2+\dot{Y}^2\right) - mg\ x\sin\alpha - MgY \tag{2.1}$$

with the dot indicating time derivative.
We impose the distance constraint by just substituting

$$(X,Y) = (\cos\alpha\ x + L\sin\theta, \sin\alpha\ x - L\cos\theta) \tag{2.2}$$

in the Lagrangian:

$$\mathcal{L}(x,\dot{x},\theta,\dot{\theta}) = \frac{m}{2}\dot{x}^2+\frac{M}{2}\left(\dot{x}^2+L^2\dot{\theta}^2+2\dot{x}\dot{\theta}L\cos(\theta+\alpha)\right)-(m+M)g\ x\sin\alpha+MgL\cos\theta \tag{2.3}$$

The Euler-Lagrange equations read, with the adjoint of external forces,

$$\frac{d}{dt}\frac{\partial\mathcal{L}}{\partial\dot{x}} - \frac{\partial\mathcal{L}}{\partial x} = Q_x \tag{2.4}$$

$$\frac{d}{dt}\frac{\partial\mathcal{L}}{\partial\dot{\theta}} - \frac{\partial\mathcal{L}}{\partial\theta} = Q_\theta \tag{2.5}$$

where the Q's are the generalized forces [Lanczos1970]. In this case, the external forces are naturally defined in the plane tangent to the manifold of Lagrange coordinates, so that the generalized forces are just, $Q_x = F_x, Q_\theta = F_\theta = -\gamma_\theta\dot{\theta}$ with no need for any projection.
Developing the derivatives, one gets the accelerations multiplied by the so called dynamical matrix $\mathcal{M}$:

$$\mathcal{M}\begin{pmatrix}\ddot{x}\\ \ddot{\theta}\end{pmatrix} = \begin{pmatrix}ML\dot{\theta}^2\sin(\theta-\alpha) - (m+M)g\sin\alpha + F_x(x,\dot{x})\\ -MgL\sin\theta + F_\theta(\dot{\theta})\end{pmatrix}, \tag{2.6}$$

$$\mathcal{M} = \begin{pmatrix}m+M & ML\cos(\theta-\alpha)\\ ML\cos(\theta-\alpha) & ML^2\end{pmatrix}. \tag{2.7}$$

After giving an explicit form for the external drive, which is the subject of the next paragraph, and initial conditions $x_0, \dot{x}_0, \theta, \dot{\theta}_0$, one can integrate numerically the equations by inverting the dynamical matrix at each step.

2.3.3 Models for the action of the wheels

The trolley slider is pushed, during its motion, against a set of $N \sim 40$ wheels with the same diameter $\Delta x \sim 50$ cm rotating at different tangential velocities v_i with $i = 1, \dots, N$. The friction between the slider and the wheels acts as a control for the trolley speed. To model the system in a simple way, we made several assumptions:

1. the distance between the tires be negligible

2. the length of the slider be exactly equal to Δx, so that at any point x of its trajectory the slider be in contact with one and only one tire $i(x)$

3. F_x be a function of only $v_{i(x)}$ and $\dot{x}$ (i.e. homogeneous friction within a section).

A simple model consists in assuming a viscous force in the frame of reference of the tire, plus a sharp cutoff at R_{max}:

$$F_x(x, \dot{x}) = -\min\{\gamma_x(\dot{x} - v_{i(x)}) \ , \ R_{max}\} \tag{2.8}$$

for $\dot{x} - v_{i(x)} > 0$ and with the max in the other case. As will be discussed in the next section, this model underestimates the drive intensity in the slow part of the track; this leads to some pathology especially when a finite slope is introduced. A more grounded proposal [Carlson2002] which takes care of this problem is to scale the value of the viscous constant by the velocity itself. In particular, defining the *slip* σ as

$$\sigma(x, \dot{x}) = -\frac{(\dot{x} - v_{i(x)})}{|\dot{x}|} \tag{2.9}$$

the force $F_x(x, \dot{x})$ is given by a function $F(\sigma \ ; F_{max})$ that is linear up to $|\sigma| \sim 0.05 - 0.1$ and then rapidly saturates to F_{max}.
The other advantage of this solution is that there are no singularities in the force expression inside a section, and for large $\dot{x}$ the expression converges to the measured maximum force, with no need of an unknown multiplicative parameter.

2.4 Analysis of the dynamics

In this section we solve the equations of motions in different regimes, to get physical insight on the role of the different factors. The most relevant reference parameters are $M = 1700$ kg, $m = 125$ Kg, $\gamma_\theta = 200$ N m , $F_{max} = 4000$ N, $\gamma_x = 4.0$ kg s^{-1}, $\dot{x}(0) = 6.0$ m s^{-1}, $L = 3.1$ m.

2.4.1 Need for two degrees of freedom

When the x trajectory is rigidly controlled by the tire velocity and the back-reaction of the cabin on the trolley does not affect the trolley motion, it is possible to speak of only 1 real degree of freedom θ. This regime is obtained in the limit m, F_{max}, $\gamma_x \to \infty$.
As apparent in Fig. (2.4), the motion is basically oscillatory and there is no dynamical stabilization of the cabin. We conclude that is fundamental to consider the back-reaction of the cabin on the trolley, then two degrees of freedom are needed.

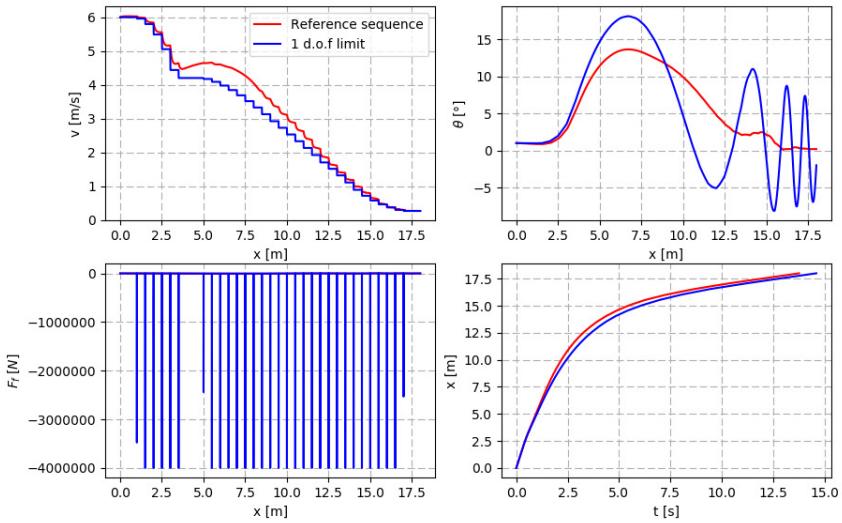

Figure 2.4: The blue line represents the situation where only 1 dof determines the dynamics, the red line serves as reference. (Top left) The plot shows the trolley velocity as function of the position. (Top right) In this panel is plotted the angle of the cabin as function of the position. (Bottom left) This plot indicates the force exerted by the tires. (Bottom right) Plot of the position as function of time.

2.4.2 Viscous versus slip model

The first consequence of having a finite slope is to reduce the load on the tires. This should allow for further optimization on the velocity array. Notice the little pathology in $x(t)$ with finite α: at the end of the track all velocities are quite small, so even large relative velocity differences $\dot{x} - v_i$ cannot dominate over the gravity force, so that there is a probably unphysical slowing down of the cabin. Increasing α can lead to the cabin never reaching the end of the track (see Fig. (2.5)). The problem can be solved by rescaling the friction coefficient by the inverse of the velocity, as shown in Fig. (2.6) below.

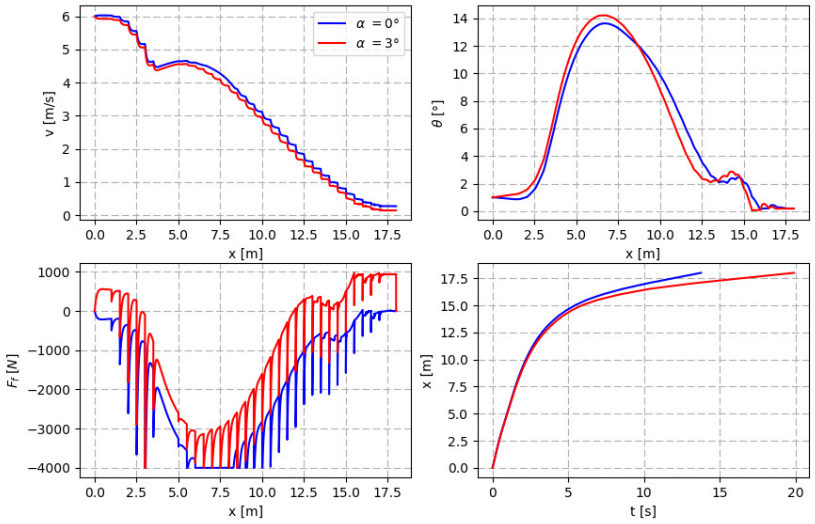

Figure 2.5: These plots show the pathology in $x(t)$ when considering finite inclination angle α and viscous model.

The slip model allows the trolley to be controlled even in the final part of the track. In this region also the angular dynamics differs from the viscous model case as plotted in Fig. (2.6).

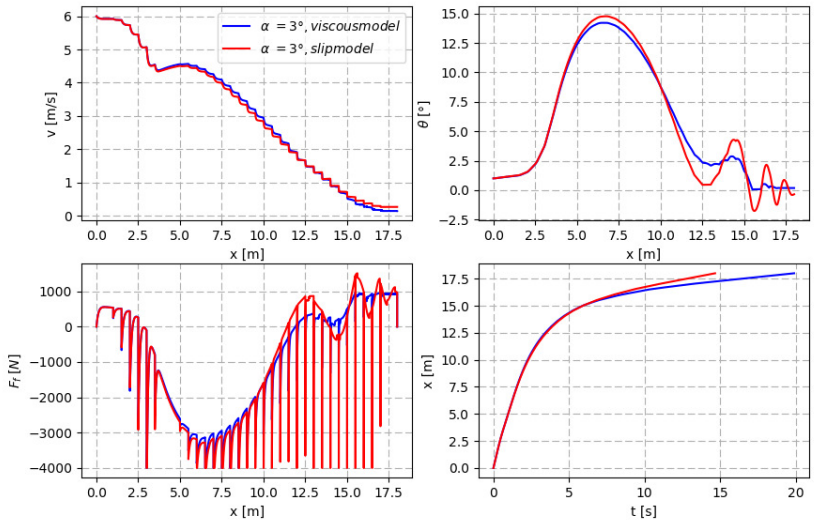

Figure 2.6: These plots highlight the difference between slip and viscous models.

2.4.3 Pseudo-optimization protocol

The simple integrator routine which solves the dynamics makes use of Euler algorithm and is written in the Julia programming language [JuliaLang].
Leitner engineers asked for a basic user interface, which allow them to interactively modify the input parameters and see the modified dynamics.
We have found an easy-to-implement, highly portable and computationally efficient hack to address Leitner requests.
The idea, sketched in Fig. (2.7) below, is to use whatever text editor to modify the text files containing the set of parameters and velocities for n trajectories (at present $n = 2$ is supported, but it is easy to generalize). Julia session contains a `while` loop with a `sleep` function that any 0.5 seconds checks the `timestamps` of the input files to see if they have been modified. In this case, the trajectories are solved with the new parameters and velocities, and the plots are updated.

2.5 Conclusions and perspectives

During the IPSP week, our team tackled the problems proposed by Leitner analyzing the system dynamics in the case where the station inclination angle is different from zero and proposing a useful tool able to optimize the parameters in order to stabilize the system.
Taking into account the limited amount of time, we considered a simple but effective mathematical model to calculate the equations of motion. In particular, the model to describe the action of the tires played a crucial role in calculating the

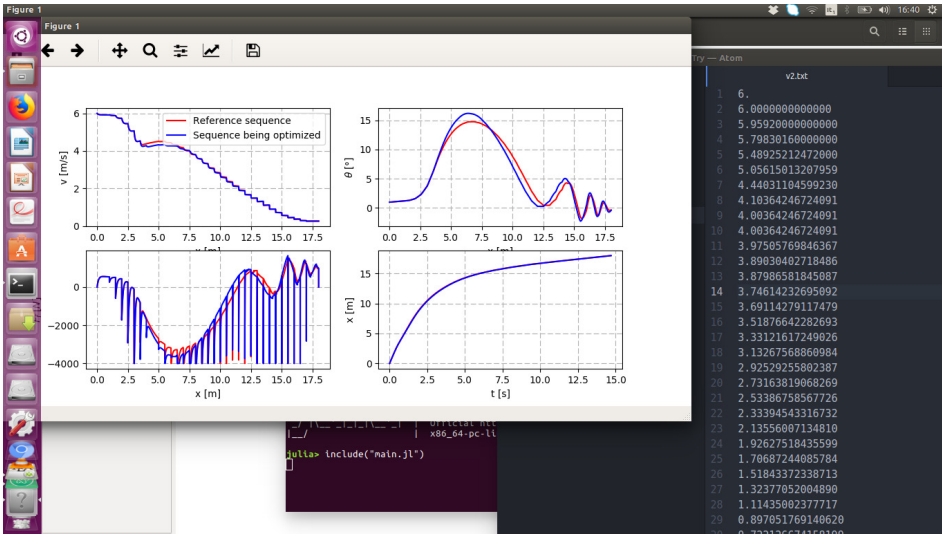

Figure 2.7: Sketch of the optimization-by-hand protocol: a Julia session is launch via the terminal, the trajectories are then plotted; any time you modify and save the input data files with your favorite editor (in this case Atom), the plots are updated. In particular, we mention that the number of wheels can be changed interactively.

right solutions (as shown in Fig. (2.5)). Once we discovered the proper model, we developed the software to solve the equations, implementing also a GUI to optimize and stabilize the cabin during the acceleration stage.
These results can be certainly improved to reach even more precise quantitative predictions. Some suggestions are listed below:

1. Study an analytical or semi-analytical treatment of the problem in a simplified regime that still gives an idea of the principle (abrupt deceleration followed by gentle acceleration and smooth deceleration again) which allows the dynamical stabilization (short-cut to adiabaticity).

2. Describe the tires in a more precise way, modifying the assumptions presented in Section (2.3.3).

3. Implement a more elaborated user interface. The only serious problem at present is that to stop the session one needs to kill it via `ctrl+C` and quit Julia.

4. Develop an optimization routine for the array of velocities v_i. The first non-trivial point is to decide a cost function for the trajectory.

Moreover, using the basic user interface described previously, we managed to obtain some optimized configurations where the number of tires was reduced, giving in such a way an idea of the potentiality of the tool developed during the IPSP event.

Bibliography

[1] C. R. Carlson and J. C. Gerdes "Identifying tire pressure variation by nonlinear estimation of longitudinal stiffness and effective radius". In Proceedings of AVEC 2002 6th International Symposium of advanced Vehicle Control, 2002.

[2] JuliaLang website: `http://julialang.org/`

[3] C. Lanczos (Ed.) (1970). *The variational principles of mechanics* (4th ed.) Dover Publications Inc. New York.

[4] J. J. W. H. Sørensen, M. K. Pederson, M. Munch, P. Haikka, J. H. Jensen, T. Planke, M. G. Andreasen, M. Gajdacz, K. Mølmer, A. Lieberoth and J. F. Sherson "Exploring the quantum speed limit with computer games". Nature, 532: 210-213, 2016.

CHAPTER

THREE

ELECTROSTATIC CHARGE ON EXTRUDED SILICONE ELASTOMER YARNS

Z. Bisadi, M. Celli, S. J. A. Lafirenze, C. Puglia, M. Singh, C. Vecchi, S. Villa

3.1 Introduction

3.1.1 The company profile

LeMur Italy Srl is a company based in Ala (TN, north of Italy) that for 20 years has been specialized in the production of single, double as well as air-jet covered spandex yarns. LeMur is a point of reference in the Italian stretch yarn market, thanks to the high quality of its products and service, the capability to satisfy every customer request, the quick delivery and the good assistance.
Moreover, 10 years ago LeMur has created the Research and Development (R&D) division to invest in a unique product. The study and research activity of the R&D staff made it possible to design and develop a worldwide-patented technology for the spinning of silicone. Thanks to this particular technology, LeMur is the first and only company able to produce the finest continuous extruded silicone profile with the dimension of a yarn. A product that is revolutionary in the field of common spandex yarns.
This silicone based elastic yarn is registered with the trademark *muriel*®. The development of different possible characteristics covers many different application fields beyond the textile industry: medical, technical and protective clothing, automotive, light management, sensor applications and food.

Figure 3.1: Silicone yarn bobbins produced by LeMur S.r.l. (left) and a family of six extruded silicone yarns just after the extruder (right).Pictures are taken from [1].

3.1.2 The problem

The production process patented by LeMur S.r.l. involves the extrusion[1] of continuous silicone elastomer yarns with diameters of a few tenths of a millimeter. Due to the high generated strain, the formation of electrostatic charges by contact is an inevitable consequence that can lead to substantial limitations during the production process. The repulsion forces generated by *triboelectric effect* may indeed be sufficient to change the motion of the yarns, causing breakages or conditioning the speed of the production process. The problem is particularly severe in the case of reduced section extruded yarn such as those produced by LeMur, which are sensitive even to the weakest stresses.
The problem has a marked relevance for the company's activity, particularly for thin yarns, that the elimination of electrostatic charges would result in an increased production capacity of the plant.
The company's requests therefore include:

- measurement of the electrostatic charges generated during the production process, with particular reference to the polarity and intensity of the charge.
- possible solutions to solve the problem, compatible with the production process developed by LeMur.

3.2 Origin of charge creation

The phenomenon of the accumulation of superficial electrostatic charge, known as triboelectricity [3] or electrification by contact [4], is common to many materials and in particular to polymers.
In the case of insulating materials and in particular for polymers, despite a widespread belief that this phenomenon is due to a process of donation/reception of electrons [5], the current scientific literature is very cautious about the

[1]Extrusion basically means physical, mechanical and chemical treatment of a material inside a restricted orifice (die) [2]. It is composed of one or two rotating Archimedes screws fitted in a barrel to successively increase the pressure and to force the material to move forward so that the expansion could take place. This type of treatment is responsible for the change of texture or shape of the initial material. So, to control this process many factors are important to consider such as size and shape of dye, screw speed, temperature and pressure.

possibility that an electronic transfer actually takes place between insulating materials characterized by the absence of valence electrons [6](Fig. 3.2.a). In fact, an exchange, and therefore an imbalance, of ionic charges at molecular level would imply a process of adhesion/adsorption of atoms or molecules during contact between two insulating objects [7] (Fig. 3.2.b).

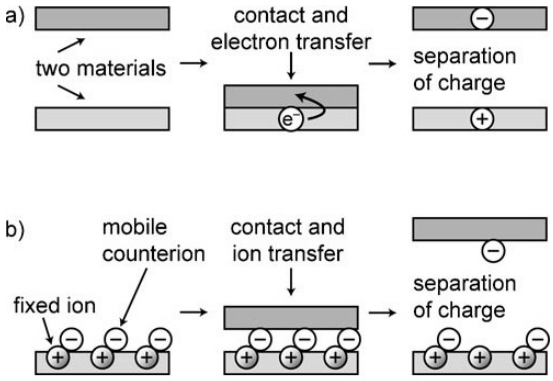

Figure 3.2: Possible mechanisms of charge transfer. a) Transfer of an electron. b) Transfer of an ion. The picture is taken from [8].

In the academic context, the case of silicone is particularly studied for some peculiarities of the material itself [9]. Pure PDMS[1] has a tendency to generate a (relatively) strong negative charge if placed in contact with a metal surface and before the vulcanization[2] can be modeled according to any geometry, even at the submicrometric level (up to molecular level). This fact is very important in the study of the formation of electrostatic charges because, allowing to model and knowing the geometric characteristics of a sample up to the nanometer level, it would be possible to understand the influence of the surface conformation and of the contact pressure in the triboelectric phenomenon [11].
From the study of the contact between two identical surfaces of PDMS-different from the metal-polymer contact occurring during spinning-it is possible to prove that the process of electrification is not one-way. This means that if the PDMS is normally charged negatively, this does not exclude the possibility that it is positively charged [11].
In fact, it is reported in literature that when two surfaces of silicone elastomer yarns are placed in contact, one loads with reverse polarity to the other. The so-called triboelectric series[3] [12] therefore prove to be of little scientific and practical value. These are indeed specific cases that result, in practice, to be impossible to generalize and apply to each case under examination.

[1]Polydimethylsiloxane

[2]Vulcanization is a chemical process for converting polymers into more durable materials by introducing cross-links (bridges). By forming cross-links between individual polymer chains, vulcanization dramatically affects the mechanical properties of a polymer [10].

[3]Lists used at the level of industrial practice which show a series of materials according to their *affinity* to be positively or negatively charged.

3.3 Charge intensity and polarity

In this section, the intensity and polarity of the charge on the extruded yarns are studied.

3.3.1 Evaluation of charge intensity

In order to evaluate the order of magnitude of the electrostatic charge density responsible for the yarns repulsion, we made simple computations based on the observations.
The external forces acting on the yarns are gravity $\vec{F}_g$ and coulomb repulsion $\vec{F}_c$, whose balance determines the equilibrium angle α between the vertical axis and the yarns (see Fig. 3.3). Here we consider the simplest case of two yarns generated by the 2-hole spinneret. Moreover, for simplicity, we evaluate the linear charge density λ considering the yarns as rigid and not deformable. In this way λ is over-evaluated.
Under such approximation the single yarn is a rigid bar bound to rotate without friction around a pin. Therefore, the two forces $\vec{F}_g$ and $\vec{F}_c$ generate a torque on the yarn ($\vec{M}_g$ and $\vec{M}_c$ respectively). The equilibrium angle α is the one for which we have:

$$\vec{M}_g + \vec{M}_c = 0 \tag{3.1}$$

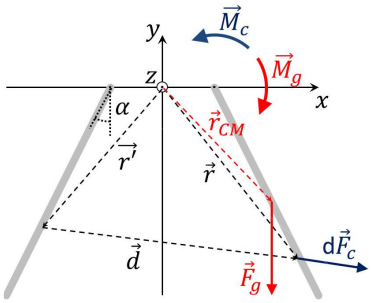

Figure 3.3: Sketch of the system of two yarns both at the equilibrium angle α as they are considered in the model for the evaluation of the electrostatic charge distribution. Considering the yarn on the right, the gravity force $\vec{F}_g$ applied on the center of mass $\vec{r}_{CM}$ generates a torque $\vec{M}_g$ in the clockwise direction, while the integral of all the infinitesimal coulomb forces $d\vec{F}_c$ between all the possible couples of points $\vec{r}$ and $\vec{r}'$ of the two yarns generates a torque $\vec{M}_c$ in the counterclockwise direction.

The torque exerted by gravity can be easily computed considering the force applied on the center of mass $\vec{r}_{CM}$ of the yarn. Naming dm the mass of an infinitesimal segment of yarn of length dl, $\vec{r}$ the coordinate of such yarn segment, and $\vec{g}$ the gravity acceleration, the torque exerted by $\vec{F}_g$ results therefore in [13]:

$$\vec{M}_g = \int \vec{r} \times \vec{g} dm \tag{3.2}$$

$$= -\rho\pi a^2 \frac{L^2}{2} g \sin\alpha \, \hat{e}_z \,, \tag{3.3}$$

where ρ is the density of the yarn, L is its length and a is the radius of its section. In the reference system depicted if Fig. 3.3, z is the axis perpendicular to the plane of the sketch and $\hat{e}_z$ is the corresponding unit vector.
For the evaluation of $\vec{M}_c$, we start by writing the coulomb repulsion between two infinitesimal segments of the two yarns of length $\mathrm{d}l$ and $\mathrm{d}l'$:

$$\mathrm{d}\vec{F}_c = \frac{\lambda^2}{4\pi\epsilon_0\epsilon_r} \frac{\vec{d}}{\left|\vec{d}\right|^3} \mathrm{d}l\mathrm{d}l' \,, \tag{3.4}$$

where ϵ_0 is the vacuum permittivity, ϵ_r the relative permittivity of the air and $\vec{d} = \vec{r} - \vec{r'}$ is the distance between the segment of the first yarn located in $\vec{r}$ and the one of the second yarn located in $\vec{r'}$. The total torque due to the electrostatic force can be then computed by double integrating $\vec{r} \times \mathrm{d}\vec{F}_c$ over $\mathrm{d}l'$ and over $\mathrm{d}l$ both from 0 to L. It has been numerically evaluated as a function of λ and α.

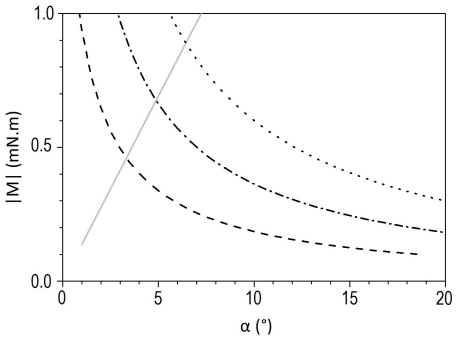

Figure 3.4: Plot of the absolute value of the torques $\vec{M}_g$ (grey) and $\vec{M}_c$ (black) versus α. The torque originated by the coulomb repulsion between the yarns is reported for different values of λ: 0.07 μC/m (dashed line), 0.07 μC/m (dash-dot line) and 0.09 μC/m (dotted line).

In Fig. 3.4 the moduli M_g and M_c are reported for different values of λ versus α. For the computation we employed the following values for the involved physical parameters. The yarn has been considered with a length $L = 1$ m. The radius of its section varies in a typical range of $0.35 - 1$ mm; we thus consider an average radius of $a = 0.675$ mm. The density of the silicone elastomer is $\rho = 1130$ Kg/m^3. The distance d_0 is the one between the two holes of the spinneret and is equal to 25 mm. The relative permittivity of the air has been evaluated considering the temperature, the relative humidity and the atmospheric pressure at Ala (TN) on

19 July 2018 at 2:00 p.m. [14]. The obtained value [15] is 1.0008 and can thus be safely approximated with 1. Figure 3.4 shows how the equilibrium angle, at which M_g and M_c intersect and the Eq. 3.1 is satisfied, increases with λ. For the measure of the equilibrium angle, α, we took a picture, reported in Fig. 3.5, of the system of the two yarns as they are when they are extruded from the spinneret with two holes. From this image the α can be evaluated in the order of 5°. Looking at Fig. 3.4 it can be seen that such angle corresponds to a linear charge density λ of the order of 0.07 μC/m. Therefore, this is the value of λ we can estimate from the model. A more precise evaluation could be made by removing the approximation of a solid bar but this is outside the present discussion as the given rough estimation is enough for the purposes of the present work.

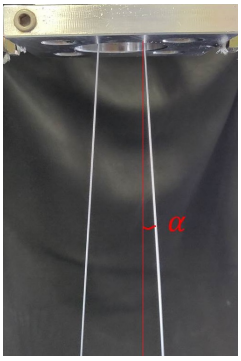

Figure 3.5: Photo of the system of two yarns as they are when they are extruded from the spinneret with two holes. The red line highlights the normal direction with respect to which the equilibrium angle α is formed.

3.3.2 Determination of charge polarity

Since the extruded yarns demonstrate a repulsion among one another, it is possible to deduce that the electrostatic charge on the yarns has the same polarity for all of them, but nothing can be said about the polarity itself.
A basic experiment to determine the polarity of the electrostatic charge could be done by placing a metallic cylinder around a single yarn. However, two problems exist: i) the charge density of about 0.07 μC/m, estimated in Section 3.3.1, is too small to induce an image charge on the metallic cylinder and ii) this experiment is difficult to be implemented in this case due to the geometrical constraint.
As an alternative, we can try to put a charged object with a known polarity near a single yarn and observe its behaviour: if it has the same sign as the charged object, it will be repelled; otherwise it will be attracted.

Van de Graaff generator

We decided to use a Van de Graaff generator [16] as the charged object in order to determine the polarity of the electrostatic charge on the extruded yarns. Therefore, first of all we needed to know the sign of the charge induced on the

top part of the generator.
A simple scheme of a Van de Graaff generator is shown in Fig. 3.6. It consists of a belt of dielectric flexible material (rubber) moving over two rollers of different materials. One of the two rollers is made of metal (the upper roller) and the other one is made of a dielectric material (the lower roller). Due to *triboelectric effect* the contact of dissimilar materials causes the rubber belt and the lower roller to become oppositely charged, i.e. the roller receives a positive surface charge and the belt a negative one. After operating for a while the belt will become weakly negative and the roller will be strongly positive due to the concentrated charge on it. The roller attracts the negative charge into the metal comb teeth placed near to it. Due to an intensely strong negative charge on the sharp metal points of the comb, the insulating air between the roller and comb is ionized and the negative charges then hit and stick to the surface of the belt. The roller rotates and the belt surface moves upwards, carrying the negative charge with it.
The upper roller made of metal, is surrounded by a hollow metallic sphere which is in contact with a metal comb positioned near the rubber at the top of the upper roller. When the field is strong enough to ionize air molecules, the positive charges are attracted by the belt, recombine with the belt negative charges and mostly cancel them out, meanwhile electrons are attracted by the comb. On the comb electrons recombine with the positive charges which exist in it. The excess charge gets spread to the outside of the terminal output or sphere. This process leaves the comb, and consequently the hollow metallic sphere, with a net charge different from zero. At the end, the hollow metallic sphere has a negative charge, as it can be seen in Fig. 3.6.

Measurements of charge polarity

While it is impossible to obtain a charge density of about 0.07 μC/m distributed in a very regular way on the surface of the yarn, it was not possible to do tests in the laboratory. So we needed to go directly to the company to perform some measurements.
As mentioned before, when we charge our Van de Graaff generator and put it near the extruded yarn two different cases are in principle possible:

- if the yarn is repelled from the Van de Graaff generator, we can say that the polarity of the charge on the yarn is the same as the polarity of the charges on the metallic sphere of the Van de Graaff generator, i.e. negative;
- if the yarn is attracted to the Van de Graaff generator, we can say that the polarity of the charge on the yarn is different from the polarity of the charges on the metallic sphere of the Van de Graaff generator, i.e. positive.

In Figure 3.7.a we observe that when we place the charged Van de Graaff generator near the extruded yarn, the generator repels the yarn. However, when we discharge the Van de Graaff generator (by touching it) the repulsion no longer exists, as can be seen in Figure 3.7.b.
Since the mechanism that causes the formation of the charge on one single extruded yarn is the same as the mechanism that causes the formation of charge

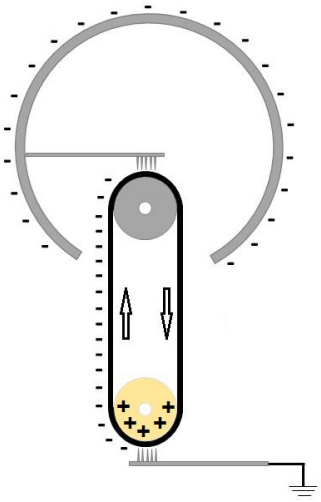

Figure 3.6: Simple scheme of a Van de Graaff generator: due to *triboelectric effect* the lower roller which is made of a dielectric material is charged positively and the rubber belt negatively. The positively-charged roller attracts the negative charge into the metal comb teeth placed near to it. A high electric field between the comb teeth and roller ionizes the air nearby and then the generated negative charges hit and stick to the surface of the belt. The roller rotates and the belt surface moves upwards, carrying the negative charge with it. At the top of the metallic roller, close to the rubber, there is the other comb in contact with the hollow metallic sphere, that is charged by the charges generated by air ionization. At the end, the net charge of the hollow sphere is negative.

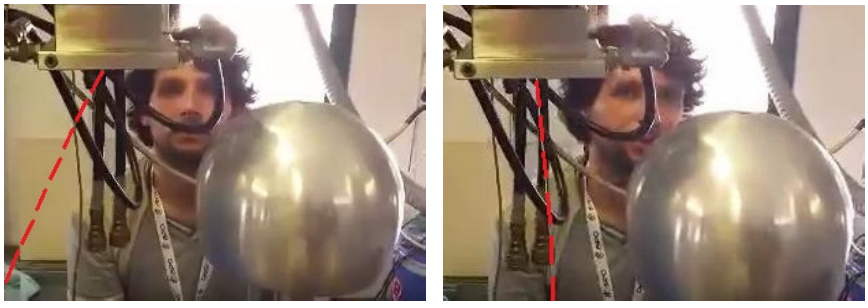

(a) Charged Van de Graaff **(b)** Discharged Van de Graaff

Figure 3.7: (a) When the Van de Graaff generator is charged it is possible to see a repulsion between the generator and the extruded yarn; (b) after the Van de Graaff generator is discharged this repulsion does not exist. The dashed red lines show the yarn which is not well-visible in the original pictures.

in all the yarns extruded together (because it depends only on the extrusion method), in the end we can say that the polarity of the electrostatic charge that are present on the surface of the extruded yarns is always negative.

3.4 Overview of possible solutions

In order to eliminate the charge from the yarns, we explored a number of possible solutions. First of all, we tried to eliminate the charge at the source, in the extrusion process. Unfortunately, it is not possible to prevent the generation of the charge due to the mechanical process of extrusion. Other possible strategies were investigated [17]:

- Photo-crosslinking: this method is based on the crosslinking of the PDMS bonds through light induction, and not through heat, as it happens during the production process. In this way, the oven is replaced by lasers, which are cost-effective. The charge is removed by the light that at the same time induces the cross-linking. The main limitations of this strategy are the modification of the production process and the low efficiency of cross-linking in very thin yarns. Instead, photo-crosslinking is already used at industry level for thick yarns.

- Faraday cage: it is a very simple and elegant solution, in which the electric charge of the yarns would be shielded by the cage. This is not feasible in our case due to practical reasons of the production process: as the yarns enter the oven they change position and due to their adhesiveness they may attach to the cages. Therefore, it would be difficult to modify the position of the cages in order to overcome this problem.

- UV-deionization: this method is based on the removal of the charges through UV exposure. UV-rays are already used to neutralize static electricity from glass and from silicon. Unfortunately, for our application a great number of lasers would be necessary and it could not be cost-effective and demanding for the production process.

- Carbon mesh: a multi-layered mesh can be used at the end point of the extruder, where the processed PDMS passes through and just before silicone yarns are formed, to filter the charges out. The mesh can be composed of different substrate, such as carbon nanotube (CNT) or graphene micro-ribbons (GMR) which result in graphene-based woven fabric (GWF). The layers of the mesh present different hole sizes, allowing the exit of the PDMS, but guaranteeing the removal of the charges. This solution needs to be implemented and tested as to find the perfect combinations of layers.

- Metal sputtering: This idea is based on the bombarding of metal cluster directly into the core of the yarn, guaranteeing its conductivity. Such conductivity would allow the discharging of the yarns. Gold is the perfect metal for this application, considering that it is also biocompatible, but the

cost would have a great impact. The main drawback of this solution is that it is necessary to build a bombarding device that should be used before the oven step. This means that, again, the production process should be modified. Moreover, the physical properties of the yarns would be altered by metal implantation.

- Screening film
- Ion blower

We focused on the last two solutions of the list, since they are most feasible based on the particular conditions of the production system and cost efficiency.

3.4.1 Screening film

The first feasible solution we decided to investigate is the screening of the electric charges by a liquid film deposited on the yarns. The possibility to avoid the divergence of the yarns without removing the electrostatic charges may be indeed obtained by changing the way the interaction decays with the distance d. The Coulomb electrostatic force is a long range interaction which scales with the square of the reciprocal of the distance ($1/d^2$), as it can be seen from Eq. 3.4. From the domain of the colloidal science, however, it is well known that if we consider the electrostatic interaction in an electrolytic liquid (instead of vacuum) the interaction is additionally modulated by a descending exponential ($\exp(-d/l_D)$). This happens because of the screening of the charges operated by the ions dissolved in the liquid [18]. As a result, the electrostatic repulsion decays much more rapidly in such case and can be considered ineffective at distances of the order of few times the Debye screening length l_D [18]. Such distance is a physical quantity defined as a function of the ions concentration present in the solution. For pure deionized water l_D is in the order of 1 μm, and decreases as the molar concentration of solutes increases. Typical values of l_D for tap water are in the order of tens of nanometers.
Our idea has been thus to coat the yarns with a film of electrolytic liquid of about a micrometer or less in order to screen the electrostatic charges. In order to do this we tried to create a film of liquid (water, water solutions or other liquid compounds) on the yarns through a nebulizer. For the first tests we did on the day we went to the company we used a commercial spray bottle but the procedure can be easily improved with more refined nebulizers.
The liquid forming the thin film must respect several constraints. It must have an autoignition point lower than 500°C (the temperature at which the yarns are vulcanized in the oven) in order to avoid the risk of explosions, and must not emanate toxic vapours because the oven is not sealed from the outside. Moreover, the liquid film should not alter the physico-chemical properties of PDMS. Importantly, in order to form a uniform film able to screen the electrostatic charges, the wettability of the yarns with the liquid must be good. In other terms, the contact angle between the liquid and the film, determined by the surface tensions through the Young's Law [19], should be low in order to guarantee the formation of a continuous film.

Liquid thin film formation

As a first test, observations have been made simply with distilled water. As we expected, due to the known hydrophobicity of PDMS, when water is sprayed on the yarn several droplets of little dimensions are formed (characteristic size of the order of hundreds of micrometers). This has been observed by naked eye, then confirmed by optical microscope. In this way, water is not so effective in shielding the electrical charges, as it does not form a continuous film and most of the electrostatic charges remain unscreened. By spraying the distilled water directly on the yarns while they were extruded, we noticed that only the deposition of a great amount of water leads to a visible effect in reducing the yarns repulsion. Unfortunately, in this case the increased weight of the yarn caused a deformation of it. We evaluated, indeed, that the weight per unit length of the yarns in this case is increased by a factor of 10: since the extruded yarns before vulcanization are still deformable, such an increment of the weight causes a thinning of the PDMS.
In order to decrease the contact angle and enhance the liquid thin film formation, we therefore decided to look for a surfactant satisfying the above mentioned characteristics for an effective production. We found in literature a paper describing the spreading of solutions of water and silicone surfactants on hydrophobic surfaces [17]. These surfactants have a molecular composition extremely similar to PDMS and respect therefore all the imposed constrains: they did not burn at the temperature of the oven and do not impact the mechanical and elastic properties of the yarn.
Moreover, these surfactants are also defined as *superspreaders*. *Superspreading agents* (or *superspeaders*) are silicone surfactants that induce water to wet hydrophobic surfaces. As a working definition, a surfactant is a superspreader if the addition of a small amount (less than 0.1%) to a small droplet of water enables it, when placed on a hydrophobic surface, to spread into a thin, wetting film within tens of seconds.
We prepared a solution using NP-40[1], a silicone-based surfactant similar to the ones described by Zhu *et al.* [17]. Two solutions were prepared with final volume of 5 mL. In the first solution, 250 μl of NP-40 were added to 4750 μl of distilled water. The second solution was prepared in the same way but adding 5 mg of NaCl in order to increase the screening by the electrolytes of the electrostatic charges of the yarn. Both the solutions have been tested on the yarn in the laboratory.
As expected, we observed the formation of an homogeneous thin film. By microscope observations, we were able to see that a single drop of 2 μl of solution spreads in a few seconds all over the yarn segment of 100 mm long, from end to end.
The prepared solutions of NP-40 are therefore able to reduce sufficiently the surface tension of the aqueous solution and thus to reduce the contact angle between the liquid and the yarn generating a continuous film. From the volume of the drop and the length of the yarn segment we recover a thickness of the film

[1] A commercial solution of NP-40 at 70% in water.

in the order of half a micrometer, corresponding to an increment of the weight of the yarn per unit length by a factor of 1.25.

Experimental screening film efficiency

After the test in the laboratory, we made a second test at the company by spraying the solutions on the extruded yarns. As in the lab, both solutions uniformly spread on the yarns and formed homogeneous thin films. The screening efficiency has been verified as adequate for our purposes, as it can be seen in Fig. 3.8. In the figure, there are reported two frames taken in the company while the yarns where extruded from the spinneret. In the first frame (Fig. 3.8.a) the yarns diverge as usual because of the electrostatic repulsion. Conversely, the second frame (Fig. 3.8.b), recorded during the spraying of the first prepared solution (distilled water and NP-40), clearly shows how the repulsion became negligible after the formation of the liquid films on the yarns. Both solutions, with and without NaCl, efficiently screened the coulomb force acting on the yarns and therefore are able to efficiently solve the company's issue.

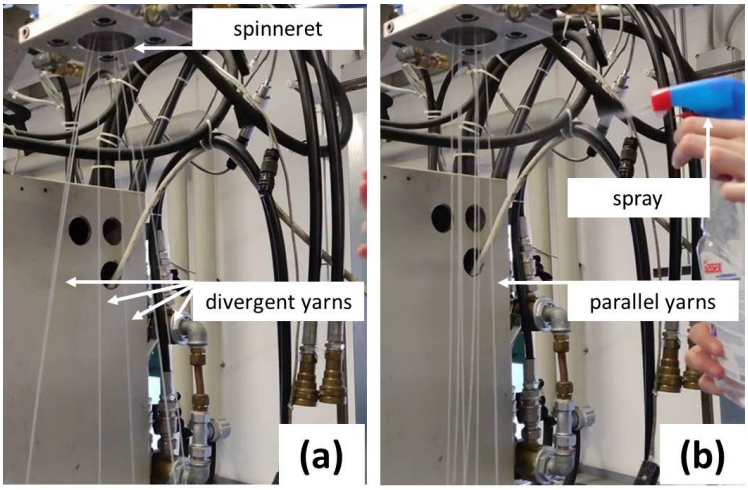

Figure 3.8: Two snapshots of the video made in the company during the extrusion of the yarns. (a) A frame recorded before the spraying of the NP-40 water solution: the yarns diverge because of the electrostatic repulsion. (b) A frame recorded while the solution was sprayed: the electrostatic repulsion is now negligible and the yarns are almost parallel.

3.4.2 Ion blower

The second feasible solution which is in fact the *physical* solution to remove the electrostatic charges on the silicone elastomer yarns is based on the use of an ion blower, a device able to create a flow of ions that once directed on the yarns neutralize the surface charge and consequently eliminate the repulsion force between the yarns.

Corona effect

The alternate voltage between the secondary circuit of the transformer and the ground generates the so-called Corona discharge on the surface of the transformer electrodes [20]. Air molecules near the surface of the electrodes are in a high electric field region, in this situation the molecules tend to be ionized due to a natural environmental event, like an ultraviolet light or cosmic ray scattering. The high electric field accelerates the ionized nucleus and the free electrons in different directions, in this way the recombination events probability decrease. Under the effect of the electric field, the electrons acquire enough energy to ionize other molecules, producing secondary electrons in a process called electron avalanche. The secondary ions production stops when the electric field is not strong enough to give the right energy to electrons [20].
Thanks to the electric field, the ions and the electrons create a "wind" of charged particles from the electrodes to the ground; this gives a directionality to the corona effect without the use of an external source.

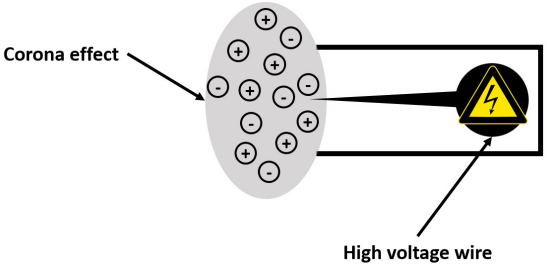

Figure 3.9: Corona effect

The ionized particles wind on the surface of the yarn neutralizes the triboelectric charges and decreases drastically the repulsion force between the yarns. It is interesting to notice that this solution works for both polarities of the charge because the ions with the same polarity of the surface charges are repulsed from the yarn.

Ionizer realization

We started evaluating two possible electrical realizations of the ion blower solution to the charged yarn problem. Indeed, among all possible ways to generate ions from the air, two are the most feasible configurations:

- The Cockcroft-Walton voltage multiplier topology;
- Tranformer-based configuration.

The basic principle behind these topologies, presented in Fig. 3.10.a and b, is the generation of a high voltage source starting from the ready to use 230V AC electrical supply. Differences between the output of these circuits are the shape of the output voltage (DC voltage from the voltage multiplier [21], AC voltage

from the transformer) and its sign (the transformer only increases the sine wave amplitude, that cross the neutral reference voltage 50 times each second, the voltage multiplier shifts the voltage up or down, depending on the configuration).

Device construction

We decided to develop the solution for the company by using the transformer, given its reduced complexity and its superior compactness. Besides, the company was already in possession of an industrial transformer that could have been used for this purpose, while all the components required for the Cockcroft-Walton voltage multiplier realization were not immediately available.
An additional advantage that maybe can be underestimated is the AC voltage at the output: this will create both positive and negative ionized particles. After the measurements, we have estimated that there is a majority of negative charges over the yarn, but there is the possibility that also positive charges can be found over the yarn, localized on certain spots. These charges cannot be eliminated by a self cancelling process with negative charges, given that the yarn has a very low conductivity. However, the AC voltage that creates both ionized particles is able to perform the removal of both charges.

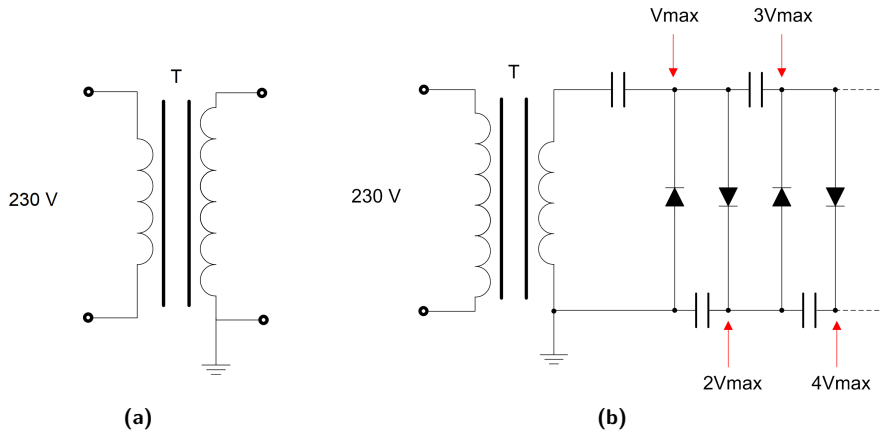

Figure 3.10: (a) Transformer and (b) Cockcroft-Walton voltage multiplier topologies. Figures are reproduced from [22].

Considering the particular shape of the extruder, the ionizer cannot be integrated in a single block. The ionizer was separated in 2 parts: the transformer part, that can be freely settled, and the nozzles block, connected together with an high voltage cable (a cable that has a strong insulation).
The transformer is a commercially available unit, with a primary-to-secondary ratio of 1:18. It is enclosed into a grounded metal box and it is provided by an overcurrent protection and by an On-Off switch.
During our measurements we have found that it is able to provide 3.93 kV RMS (11.125 kV peak-to-peak), about the theoretical maximum voltage, that

is sufficient to ionize the air.
Our purpose is to develop a device that is able to exploit the corona effect in order to ionize the air. To obtain the maximum effect, we want also to take advantage of the tip effect, using a very sharp needle connected to the transformer. The ground reference is directly taken from the extruder, that is grounded. However there was the necessity to use an interface between the extruder and the nozzles that can also hold in position the nozzles themselves. So we have recycled a metallic interface present in the company, that is in direct contact with the extruder, when connected to it.
We also decided to screen the needles from the grounded interface, in order to prevent the arcing phenomenon. The screen was realized through an hollow metallic cylinder connected to the interface through insulating bolts, so it remains to a floating potential. This nozzle has 2 additional functionalities:

1) It holds in position the needle connected to the high voltage cable, indeed it incorporates 2 holes, in which the high voltage cable can pass;

2) Its hollow structure is suitable to a connection with a pneumatic system that could inject an air flow that transports the ionized particles closer to the yarn and increases the performances, if required.

In order to distribute the ionized particles in a uniform way we built the structure by using 4 nozzles (made of aluminum with an iron needle inside) organized in circle, all around the yarn (Fig. 3.11). After having fixed them to the interface, we shoved the cable into the dedicated holes and we have inserted with pressure the needles into the cable, putting them in contact with the conductor. They should not touch the cylinder, so we centered them and fixed with epoxy. The particular shape of the nozzles boosts the particles beam like a gun, in this way we can aim the flow of ions on the yarns.
We managed to have one visit to the company in order to test the ionizer directly on the field. After the ionizer settlement on the machine, we started to extrude the yarn in order to see if the ionizer is effective.
The extrusion process is usually very difficult at the beginning, because the weight of the yarn is really low and it cannot compensate the repulsive effect and therefore the yarn sticks to everywhere. However, with the ionizer in action, the extrusion from the beginning was optimum and all the yarns were perfectly parallels, without any repulsive phenomenon. Furthermore, the ionizer was powerful enough to discharge the yarns without using the optional airflow. In any case, the airflow can be implemented when the ionizer will be used in a production line with an higher number of yarns.

3.5 Conclusions

The problem of the generation of an electrostatic surface charge density is a well-known problem in industrial processes for the extrusion of elastomer yarns. In the problem proposed by the company, the repulsion between silicon elastomer yarns does not allow an effective production of particularly low diameter yarns.

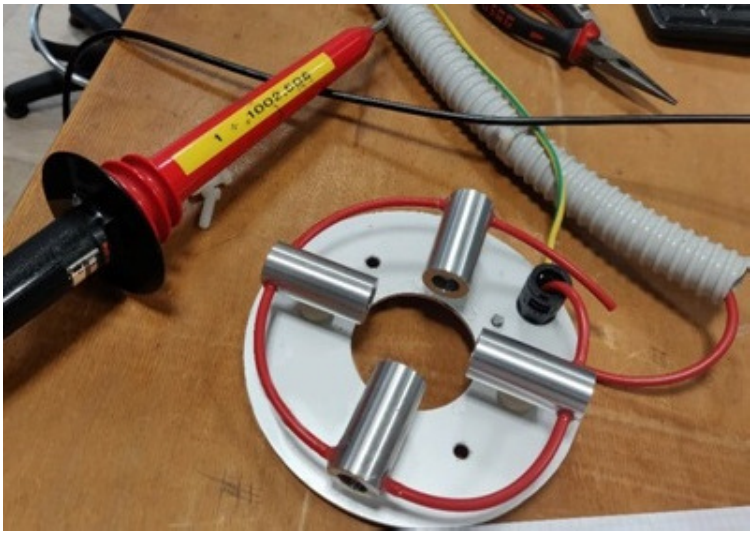

Figure 3.11: Ionizer configuration

To solve the problem we first studied the system from an electrostatic point of view; modelling two yarns with linear charge density we estimated the modulus of the charge. In addition, thanks to a negatively charged Van de Graaff generator we were able to know the polarity of the charge.
Afterwards, we designed and implemented two of the feasible solutions we thought of. The "chemical" one consists in spraying a proper solution on the yarns in order to create a shielding layer on the surface as in this way the repulsive force between the yarns is drastically reduced.
The "physical" one instead is the use of an ion blower, a device able to create a flow of ions that we direct on the yarns in order to neutralize the surface charge. Finally, we tested both solutions on the experimental production line of the company getting excellent results. The company was very satisfied with the obtained results and has implemented the physical solution on the main production line so far.

Bibliography

[1] `http://lemur-italy.com/it/azienda/`

[2] P. G. Lafleur, B. Vergnes (Eds.)(2014). *Polymer extrusion.* John Wiley & Sons.

[3] A. F. Diaz and R. M. Felix-Navarro "A semi-quantitative tribo-electric series for polymeric materials: the influence of chemical structure and properties". Journal of Electrostatics, 62(4): 277-290, 2004.

[4] H. Izadi, K. M. E. Stewart, and A. Penlidis "Role of contact electrification

and electrostatic interactions in gecko adhesion". Journal of the Royal Society Interface, 11(98): 20140371, 2014.

[5] R. A. Lodge and B. Bhushan "Effect of physical wear and triboelectric interaction on surface charge as measured by Kelvin probe microscopy". Journal of colloid and interface science, 310(1): 321-330, 2007.

[6] M. W. Williams "Triboelectric charging of insulators – Mass transfer versus electrons/ions". Journal of Electrostatics, 70(2): 233-234, 2012.

[7] M. W. Williams "Triboelectric charging in metal–polymer contacts–How to distinguish between electron and material transfer mechanisms". Journal of Electrostatics, 71(1): 53-54, 2013.

[8] L. S. McCarty and G. M. Whitesides "Electrostatic charging due to separation of ions at interfaces: contact electrification of ionic electrets". Angewandte Chemie International Edition, 47(12): 2188-2207, 2008.

[9] B. N. J. Persson, M. Scaraggi, A. I. Volokitin, M. K. Chaudhury, and P. Gr "Contact electrification and the work of adhesion". EPL (Europhysics Letters), 103(3): 36003, 2013.

[10] J. E. MARK, B. Erman and M. Roland (Eds.)(2005). *The science and technology of rubber*. p. 768. Academic press.

[11] M. M. Apodaca, P. J. Wesson, K. J. M. Bishop, M. a Ratner, and B. a Grzybowski "Contact electrification between identical materials". Angewandte Chemie International Edition, 49(5): 946-949, 2010.

[12] C. H. Park, J. K. Park, H. S. Jeon, and B. C. Chun "Triboelectric series and charging properties of plastics using the designed vertical-reciprocation charger". Journal of Electrostatics, 66(11-12): 578-583, 2008.

[13] P. Mazzoldi, M. Nigro, and C. Voci (Eds.)(2008) *Elementi di Fisica: meccanica e termodinamica*. 2nd Edition. Edises.

[14] Source of the data: `http://www.alameteo.it/`

[15] M. S. Zarnik, and D. Belavic "An Experimental and Numerical Study of the Humidity Effect on the Stability of a Capacitive Ceramic Pressure Sensor". Radioengineering, 21(1): 201-206, 2012.

[16] R. J. Van De Graaff, K. T. Compton and L. C. Van Atta "The electrostatic production of high voltage for nuclear investigations". Physical Review, 43(3): 140-–157, 1933.

[17] S. Zhu, W. G. Miller, L. E. Scriven, and H. T. Davis "Superspreading of water–silicone surfactant on hydrophobic surfaces". Colloids and Surfaces A: Physicochemical and Engineering Aspects, 90(1): 63-78, 1994.

[18] R. J. Hunter (Ed.) (2001), *Foundations of Colloid Science*. Oxford University Press.

[19] T. Young “III. An essay on the cohesion of fluids”. Philosophical transactions of the royal society of London, 95: 65-87, 1805.

[20] M. A. Goldman and R. S. Sigmond “The corona discharge, its properties and specific uses”. Pure and Applied Chemistry, 57(9): 1353-1362, 1985.

[21] N. M. Waghamare and R. P. Argelwar “High voltage generation by using Cockcroft-Walton multiplier”. International Journal of Science, Engineering and Technology Research (IJSETR), 4(2): 256-259, 2015.

[22] M. Patrignani, Duplicatore e moltiplicatore di tensione a diodi e condensatori per alimentazione anodica, `www.audiovalvole.it`.

CREDITS

The entire group on the opening day

From left to right, front row: Zahra Bisadi, Matteo Di Giovanni, Chiara Vecchi, Michele Celli, Ivan Amelio, Jacopo Nespolo, Anup Saha, Claudio Puglia, Michele Salvagni, Alberto Nardin.

From left to right, second row: Sofia Colombi, Simona Jole Anna Lafirenze, Manjot Singh, Davide Bazzanella, Sandro Huber, Ernest Miorando (*Ducati Energia*), Lucio Boscolo (*Ducati Energia*), Dario Zeni (*LeMur S.r.l*), Alessandro Santini (*Confindustria Trento*), Lorenzo Pavesi (*Department of Physics, UniTrento*).

From left to right, back row: Massimiliano Rozza (*Alternanza Scuola-Lavoro*), Roghieh Haghani, Veronica Barchetti (*HIT*), Andrea Morvisoni (*Trentino Sviluppo*), Christian Giacom (*Trentino Sviluppo*), Claudio Tonetta (*Leitner Ropeways*), Klaus Erharter (*Leitner Ropeways*), Riccardo franchi, Daniele Scappini, Matteo Endrizzi, Stefano Villa, Niccolò Tubini, Lucia Verin (*LeMur S.r.l*), Massimo Eccel (*Divisione Supporto Ricerca Scientifica e Trasferimento Tecnologico, UniTrento*), Luca Baglivo (*Trentino Sviluppo*), Claudio Nidasio (*Alumnus of Divisione Supporto Ricerca Scientifica e Trasferimento Tecnologico, UniTrento*), Adriano Zanfei (*Ducati Energia*), Maurizio Scalet.

Foto Giuseppe Froner - Archivio Università degli Studi di Trento

Ducati Energia team

From left to right: Zahra Bisadi, Matteo Di Giovanni, Sofia Colombi, Niccolò Tubini, Ernesto Miorando, Riccardo Franchi, Davide Bazzanella, Maurizio Scalet, Michele Salvagni, Alberto Nardin, Jacopo Nespolo, Lucio Boscolo, Adriano Zanfei.

Foto ©LucaValenzin per UniTrento

Leitner Ropeways team

From left to right: Roghieh Haghani, Zahra Bisadi, Sofia Colombi, Matteo Di Giovanni, Sandro Huber, Ivan Amelio, Anup Saha, Daniele Scappini, Matteo Endrizzi, Claudio Tonetta.

Foto ©LucaValenzin per UniTrento

LeMur Italy team

From left to right, front row: Chiara Vecchi, Simona Jole Anna Lafirenze, Manjot Singh.

From left to right, back row: Zahra Bisadi, Sofia Colombi, Matteo Di Giovanni, Claudio Puglia, Mario Dorighelli, Michele Celli, Stefano Villa, Dari Zeni.

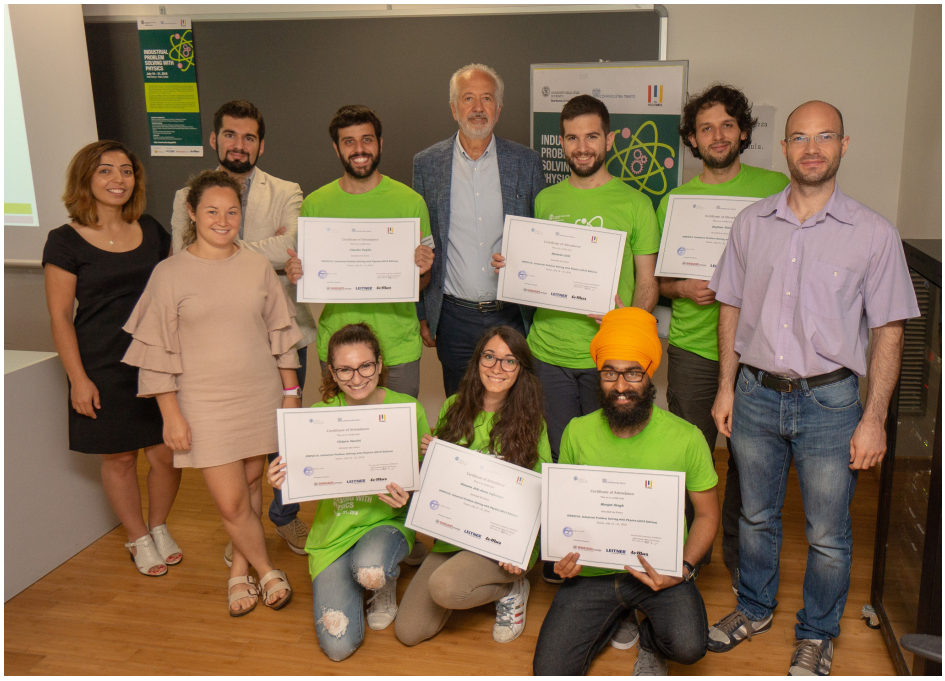

Foto ©LucaValenzin per UniTrento

ACKNOWLEDGMENTS

We acknowledge the Department of Physics, the Doctoral School in Physics, the Research and Technology Transfer Support Division of the University of Trento, Confindustria Trento and Trentino Sviluppo – Polo Meccatronica, and also the Contamination Lab Trento where the presentation of the results of IPSP2017 and the launch of IPSP2018 were held. We are particularly grateful to Prof. Lorenzo Pavesi for the constant interest in the initiative, for all the advice and support.
We would also like to thank Vanessa Ravagni, Claudio Nidasio, Massimo Eccel and Lino Giusti for their precious help during the organization of the event and in the field of intellectual properties. Many thanks to Alessandro Santini, that assisted us in finding some potential participating companies. We are grateful to Paolo Gregori, for his commitment to involve the companies belonging to Polo Meccatronica. We also thank Dr. Alessandro Rossi and Gloria Cannone for helping us in the promotion of the event.
We extend special thanks to all the companies which believed in this project and decided to nominate themselves. In particular, our thanks go to the participant companies: Ernesto Miorando, Adriano Zanfei, Lucio Boscolo from Ducati Energia, Klaus Erharter and Claudio Tonetta from Leitner Ropeways, and Dario Zeni and Mario Dorighelli from LeMur S.r.l. whose interesting and challenging inputs make this event possible. IPSP would not have certainly been possible without the enthusiasm of the students and researchers who decided to join us in this adventure. Thank you for your fundamental contribution.
We also would like to thank Martina Lorenzi from the Communication Office - Polo Collina of the University of Trento, the staff of the Laboratori Didattici, Department of Physics, University of Trento, who made their instrumentation, laboratories and personal knowledge available throughout the week. A precious help came also from Zahra Bisadi, who committed herself to the success of every details, from the most insignificant to the most important.
Finally, thank to all the people who decided to support us in the realization of Industrial Problem Solving with Physics, edition 2018.

Sofia Colombi, Matteo Di Giovanni
Sientific Committee of IPSP2018

Industrial Problem Solving with Physics (IPSP) is a one-week event organized by the Department of Physics, the Doctoral Programme in Physics and the Research Support and Knowledge Transfer Division of the University of Trento, in collaboration with Confindustria Trento and Polo Meccatronica - Trentino Sviluppo.

3 companies and 30 brains (master students, PhD students and research fellows) are selected and work together to find solutions to practical industrial problems proposed by the participating companies.

Young and motivated researchers have the chance to show off their skills in tackling new practical challenges. The participating companies, on the other hand, obtain solutions to their problems and experience an alternative problem solving strategy.

SCIENTIFIC COMMITTEE

Sofia Colombi, Department of Physics
Matteo Di Giovanni, Department of Physics

ADVISORY BOARD

Lorenzo Pavesi, Department of Physics
Giovanni Andrea Prodi, Doctoral Programme in Physics
Vanessa Ravagni, Research and Technology Transfer Support Division
Alessandro Santini, Confindustria Trento
Paolo Gregori, Polo Meccatronica

event.unitn.it/ipsp2018

Participant companies

LEITNER® ropeways

DUCATI energia
C.R.D. Centro Ricerche Ducati Trento

leMur ITALY

ISBN 978-88-8443-823-2